REPORT DOCUMENTATION PAGE

AFRL-SR-AR-TR-09-0212

1. AGENCY USE ONLY (Leave blank)	2. REPORT DATE 3. Feb. 9, 2009	3. REPORT TYPE AND DATES COVERED Final; October 1, 200S - November 14, 2008 with no-cost extension until May 14, 2009

4. TITLE AND SUBTITLE Radar Imaging and Target Identification	5. FUNDING NUMBERS 6. FA9550-06-1-0017
6. AUTHOR(S) Margaret Cheney	
7. PERFORMING ORGANIZATION NAME(S) AND ADDRESS(ES) Rensselaer Polytechnic Institute 110 Eighth Street Troy, NY 12180	8. PERFORMING ORGANIZATION REPORT NUMBER
9. SPONSORING / MONITORING AGENCY NAME(S) AND ADDRESS(ES) Air Force Office of Scientific Research ATTN: Dr. Arje Nachman-NE 875 North Randolph Road Ste 325, Room 3112 Arlington, VA 22203	10. SPONSORING / MONITORING AGENCY REPORT NUMBER
11. SUPPLEMENTARY NOTES	

12a. DISTRIBUTION / AVAILABILITY STATEMENT unlimited distribution	12b. DISTRIBUTION CODE

13. ABSTRACT (Maximum 200 Words)

This project dealt with radar remote sensing problems, including radar systems involving multiple transmitters and receivers, and the identification of targets in a complex environment. The project developed various imaging algorithms similar to synthetic-aperture radar.

14. SUBJECT TERMS radar imaging, synthetic-aperture radar (SAR)	15. NUMBER OF PAGES 16. PRICE CODE

17. SECURITY CLASSIFICATION OF REPORT	18. SECURITY CLASSIFICATION OF THIS PAGE	19. SECURITY CLASSIFICATION OF ABSTRACT	20. LIMITATION OF ABSTRACT
unclassified	unclassified	unclassified	unlimited distribution

Final Report
Radar Imaging and Target Identification
AFOSR Grant FA9550-06-1-0017

October 1, 2005 - November 14, 2008
with no-cost extension until May 14, 2009

Principal Investigator: Margaret Cheney
Department of Mathematical Sciences
Rensselaer Polytechnic Institute
Troy, NY 12180
cheney@rpi.edu

February 9, 2009

Contents

Chapter 1

Project description

1.1 Objectives

This project deals with radar remote sensing problems, including foliage-penetrating synthetic-aperture radar (SAR), radar systems involving multiple transmitters and receivers, and the identification of targets in a complex environment.

1.2 Personnel supported on this contract

1.2.1 Faculty

Margaret Cheney (Principal Investigator)

1.2.2 Postdoc

One month of support was charged to this contract for our postdoc Trond Varslot, who had been working with us for more than a year on a DARPA project. He is now at the Australian National University.

1.2.3 Consultant

Liz Rachele was paid $5k as a consultant. She has a math Ph.D. from the University of Washington (advisor Gunther Uhlmann) and was an assistant

professor at Tufts for a few years. She is now living in the area for personal reasons and is working with us on these projects.

1.2.4 Graduate students

- Hector Morales , citizen of Mexico, Ph.D. December 2008. Thesis title: "Synthetic-Aperture Radar Imaging and Waveform Design for Dispersive Media". Stipend and tuition were charged to this contract for two years; in the last year only stipend and registration-in-absentia fees were charged.

- Yi Fang, citizen of China, Ph.D. December 2008. Thesis title: "Imaging from Sparse Measurements". One year of stipend and registration-in-absentia fees were charged to this contract.

- Heather Palmeri's stipend and tuition for the spring of 2009 are being charged to this contract. Heather (a U.S. citizen) is in our accelerated B.S./Ph.D. program.

1.3 Other members of our RPI research group

The following were NOT supported under this contract, but were involved in some of the work.

- Prof. Birsen Yazıcı, Electrical, Computer, and Systems Engineering Dept.

- Graduate student supported by SMART fellowship: Matt Ferrara, Ph.D. May 2006, now in RYAT. Thesis title: "Radar Signal Processing".

- Postdoc supported by China Scholarship Council: Dr. Ling Wang

- Postdoc funded by Prof. Yazıcı: Dr. Venky Krishnan. He is a former student of Gunther Uhlmann's and wrote a dissertation on microlocal analysis. After a postdoc at Tufts, he took a postdoctoral position here at RPI and is funded by Birsen Yazıcı.

- **Other Math graduate students**

  - Analee Miranda, a US citizen, is currently funded on a fellowship from RPI. We are seeking funding for her to finish her degree.
  - Kaitlyn Voccola, a US citizen, is supported by ATR Center grant from AFRL.

- **Current undergraduate student**
  - Tegan Webster, a US citizen, joined us in Spring 2009

Chapter 2

Interactions/Transitions

2.1 National Research Council Fellowship

I received a fellowship from the National Research Council to spend time at AFRL, and spent the first 6 months of 2007 at Wright-Patterson. I renewed the fellowship for a 3-month period during the summer of 2008, which I split between RYRT in Rome and RYAT in Wright-Patterson.

2.2 Other Visits to AFRL

In addition to the NRC-supported time I spent at Rome and Wright-Patterson, I have also been stopping in for several shorter visits to both labs and have also visited Richard Albanese a half-dozen times at Brooks. For some of the latter visits, I have brought with me Birsen Yazıcı, Liz Rachele, and/or Matt Ferrara.

2.3 Summer jobs for students

- As part of his SMART fellowship, Matt Ferrara spent the summer of 2006 in RYAT at Wright-Patterson, where he remained in the fall to finish his dissertation and where he has remained since.
- For the summer of 2008, I arranged for Analee Miranda to work at Science, Engineering, and Technology (SET) Corp. She worked on

the Counterbomber project, a Doppler system for detecting explosive carried by pedestrians.

- I arranged for Heather Palmeri to spend the summer of 2008 at AFRL (Rome) in RYRT. She helped to troubleshoot the indoor radar tomography system.
- Katie Voccola spent the summer of 2008 at RYAT as part of her ATR Center work. She worked on statistical approaches to identifying lines from SAR data.
- I helped arrange an offer from MITRE for Dan Erceg for the summer of 2008; he went instead to the NSA and is now teaching high school in the Kingston (NY) area.

2.4 Efforts to bring the math community together with the radar signal-processing community

2.4.1 Organization of the SIAM Imaging Science conference 2008

In 2006, I was elected Program Director of the SIAM imaging Science Activity Group, which meant that I was responsible for organizing the 2008 Imaging Science conference. I chose as co-organizer Gary Hewer, of the Naval Air Warfare Center Weapons Division. The conference took place in San Diego in July of 2008, and included a plenary talk on radar imaging, a minisymposium on the same topic, sessions organized by the National Geospatial Agency, and panels of program managers. Participants seemed to be generally very happy with the conference.

2.4.2 CBMS Lecture Series and Monograph

Tuncay Aktosun (University of Texas at Arlington) received a grant from the Conference Board on the Mathematical Sciences for me to give a series of 10 lectures on radar imaging during May of 2008. Part of CBMS arrangement

is that the lectures should be written up as a short monograph; the final version has been delivered to SIAM for publication.

2.4.3 Plenary talk at the International Congress of Industrial and Applied Mathematics

In July of 2007, I gave a plenary talk on radar imaging at ICIAM in Zurich. It was well-received.

2.4.4 Ten-Lecture Tutorial at the IMA

In September 2005, I gave a 10-hour series of tutorial lectures on Radar Imaging at the Institute for Mathematics and Its Applications, Minneapolis.

2.4.5 Other talks and conference participation

Invited talks

- October 28, 2008, "Radar Imaging with Temporal, Spectral, and Spatial Diversity", Forty-Second Asilomar Conference on Signals, Systems, and Computers, Asilomar, CA.
- June 11, 2008, "Radar Imaging with Temporal, Spectral, and Spatial Diversity", Mathematical Methods in Wave Propagation, Växjö, Sweden.
- February 19, 2008, "Radar Imaging", math colloquium, Brigham-Young University.
- January 31, 2008, "Waveform Design for Radar Detection and Imaging", SAMSI Workshop on Imaging Problems, Research Triangle Park, NC.
- December 13, 2007, "Waveform Preconditioning for Clutter Rejection", Computational Advances in Multi-Sensor Adaptive Processing, St. Thomas, U.S. Virgin Islands.
- December 6, 2007, "Waveform Design for Radar Detection and Imaging", Technology Service Corporation, Silver Spring, Maryland.

- August 20, 2007, "Imaging Moving Targets from Scattered Waves", Unifying Framework Workshop, Gordon Center for Subsurface Sensing & Imaging Systems, Northeastern Univ., Boston.
- March 11, 2007, "Synthetic-aperture radar imaging", Air Force Institute of Technology, Wright-Patterson AFB, Dayton, OH
- February 8, 2007, "Overview of my radar research", Sensors directorate, Wright-Patterson AFB, Dayton, OH
- December 18-20, 2006, two lectures: "Radar imaging: Synthetic-Aperture Radar", and "Waveform Design for Radar Detection and Imaging", Workshop on Sensors, Signals, and Scheduling, Adelaide/Melbourne, Australia
- July 25, 2006, "Microlocal analysis and radar imaging", at Unifying Framework Workshop, Gordon Center for Subsurface Sensing & Imaging Systems, Northeastern University, Boston.
- May 17, 2006, "Resolution issues in radar and x-ray CT", SIAM Imaging Science meeting, Minneapolis
- May 16, 2006, "Doppler-only synthetic-aperture imaging", SIAM Imaging Science meeting, Minneapolis
- May 16, 2006, Minitutorial: "Introduction to Radar Imaging: Inverse Synthetic Aperture Radar", SIAM Imaging Science meeting, Minneapolis
- May 12, 2006, "Radar imaging and waveform design", EE Dept., Arizona State
- March 24, 2006, "Radar imaging and Waveform design", Workshop on Time Domain Analytic Methods, Wright-Patterson AFB, Dayton, OH.
- January 14, 2006, "Imaging that exploits multipath scattering", Combined Mathematics Meetings, San Antonio, Texas.
- January 13, 2006, "Doppler-only Synthetic Aperture Imaging", Combined Mathematics Meetings, San Antonio, Texas.
- December 13, 2005, "Radar Imaging", Honeywell, Minneapolis.

- October 27, 2005, "Radar Imaging", Applied Mathematics Seminar, University of Minnesota.

Other conference participation

- Attended AFRL/RYAT Industry Day, Dayton, OH, Dec. 3, 2008.
- Attended DARPA workshop on urban wave propagation, Arlington, VA, July 15-16, 2008.
- Attended EUSAR conference, June 2-5, 2008, Friedrichshafen, Germany.
- Contributed lecture: "Imaging that exploits spatial, temporal, and spectral aspects of far-field radar data", March 18, 2008, SPIE Defense & Security Conference, Orlando, FL.
- Participant: Sensors Technology Algorithm Research (STAR) Workshop, July 25-26, 2007, Wright-Patterson Air Force Laboratory, Dayton, OH.
- Invited Poster: "Microlocal Methods in Inverse Synthetic Aperture Radar", ATR Center kickoff meeting, Jan. 7, 2007, Dayton, OH.
- Participant: Surface Surveillance Technology, October 23, 2007, Lincoln Laboratory, Boston.
- Invited poster: Defense Applications of Signal Processing, Dec. 11-14, 2006, Fraser Island, Australia.
- Industry Day, Automatic Target Recognition Directorate, Wright-Patterson AFB, Nov. 29, 2006.
- Invited particpation: DARPA Urban Wave Propagation workshop, Oct. 4-5, 2006, San Diego, CA
- Poster: "Waveform design for SAR", Adaptive Signal Array Processing, June 6-7, 2006, Lincoln Labs, Lexington, MA
- Poster: "Microlocal ISAR for low singal-to-noise environments", IEEE Radar conference, April 24-26, 2006, Verona, NY.

2.4.6 Editorial work

- 2004 - 2007: Member of AMS Editorial Boards Committee
- 1998 - present: Member of editorial board for Inverse Problems
- 2006 - present: Member of editorial board for new AIMS journal Inverse Problems and Imaging
- 2007 - present: Member of editorial board for new SIAM Journal on Imaging Science
- 2008 - present: Member of editorial board for IEEE Transactions on Image Processing

Chapter 3

Technical Results

3.1 Publications

3.1.1 Book manuscript submitted

"Fundamentals of Radar Imaging", M. Cheney and B. Borden, SIAM.

This book explains the fundamentals of radar imaging to a mathematical audience. We hope that this book will enable mathematicians to begin work in radar imaging.

3.1.2 Journal Papers

1. "Synthetic-aperture imaging from high-Doppler-resolution measurements", B. Borden and M. Cheney, Inverse Problems 21 (2005) 1-11.

   This paper develops an alternative SAR-like image formation process requiring that only a single frequency be transmitted from a moving antenna.

2. "Enhanced angular resolution from multiply scattered waves", C.J. Nolan, M. Cheney, T. Dowling, and R. Gaburro, Inverse Problems 22 (2006) 1817-1834.

   This paper addresses SAR in the case of a target near a vertical wall that is causing multipath scattering. The analysis unfortunately requires narrow beams that either undergo multipath scattering or undergo only direct scattering, but not a combination of both. In other

words, the antenna beam cannot illuminate the corner where the vertical wall meets the ground.

3. "Synthetic Aperture Inversion in the Presence of Noise and Clutter", B. Yazici, M. Cheney, and C.E. Yarman, Inverse Problems 22 (2006) 1705-1729.

   This paper develops the theory needed for explicitly addressing noise and clutter in the imaging process. This is one of the first papers to combine statistics and microlocal analysis.

4. "A variational approach to waveform design for synthetic aperture imaging", T. Varslot, C.E. Yarman, M. Cheney, B. Yazici, Inverse Problems and Imaging, 1 (2007) 577-592.

   This paper applies the statistical/microlocal theory of item 3 to the problem of designing waveforms to suppress clutter.

5. "Wideband pulse-echo imaging with distributed apertures in multipath environments", T. Varslot, B. Yazici, and M. Cheney, Inverse Problems 24 (2008) 045013.

   This paper develops a Hilbert-space approach to multistatic radar imaging. One advantage of this approach is that multiple sensors can transmit simultaneously. Another advantage is that the method lends itself to distributed computation and efficient communication between sensors.

6. "Bistatic Synthetic Aperture Radar Imaging for Arbitrary Flight Trajectories", C.E. Yarman, B. Yazici, and M. Cheney, IEEE Trans. Image Processing, Vol. 17 (2008) No: 1, pp: 84-93.

   The theory of bistatic radar imaging is a straightforward extension of our microlocal approach to monostatic SAR.

7. "Imaging Moving Targets from Scattered Waves", M. Cheney and B. Borden, Inverse Problems 24 (2008) 035005.

   This paper shows how to combine the temporal (time delay), spectral (Doppler), and spatial aspects of radar data. It shows how it may be possible to form images of moving targets.

This paper was posted in early April 2008. In late April this paper was selected for inclusion in IoP Select; this selection is based on the criteria

- Substantial advances or significant breakthroughs
- A high degree of novelty
- Significant impact on future research

By the end of May, this article had been downloaded 250 times. (Across all IoP journals, only 10% of articles were downloaded over 250 times during the first quarter of 2008.) As of Dec. 1, it had been downloaded 500 times. (Across all IOP journals, only 3% of articles were accessed over 500 times in 2008.)

3.1.3 Journal Papers submitted

- "Multistatic Radar Imaging of Moving Targets", L. Wang, M. Cheney, B. Borden, submitted to IEEE Trans. Aerospace & Electronic Systems, Dec. 2008.

  This paper shows simulations corresponding to the theory developed in item 7 above. Surprisingly, it shows that for certain geometries, it may be possible to simultaneously determine location and velocity of a distribution of moving targets.

- "Time-reversal Waveform Preconditioning for Clutter Rejection using Distributed Apertures in Multi-path Environment", T. Varslot, B. Yazici, M. Cheney, submitted to special MIMO issue of IEEE Journal of Selected Topics in Signal Processing, February 2009.

  This paper shows how a time-reversal process can be used to adaptively determine clutter-rejecting waveforms.

- "Identification of Multiple-Scattering Events from 3D GTD-Based Parametric Scattering Models" by Matthew Ferrara, Margaret Cheney, and Gregory Arnold, submitted to IEEE Trans. Aerospace & Electronic Systems, March 2008.

  This was work from Matt Ferrara's dissertation.

3.1.4 Conference Proceedings and Book Chapters

- "Microlocal analysis of GTD-based SAR models", M. Cheney and B. Borden, in Algorithms for Synthetic Aperture Radar Imagery XII, ed. E.G. Zelnio and F.D. Garber, SPIE Proceedings series vol. 5808 (SPIE, Bellingham, WA, 2005), pp. 15-23.

- "Doppler-only imaging of stationary targets", B. Borden and M. Cheney, in Algorithms for Synthetic Aperture Radar Imagery XII, ed. E.G. Zelnio and F.D. Garber, SPIE Proceedings series vol. 5808 (SPIE, Bellingham, WA, 2005), pp. 132-141.

- "Imaging that exploits multipath scattering from point scatterers", M. Cheney and R.J. Bonneau, in Algorithms for Synthetic Aperture Radar Imagery XII, ed. E.G. Zelnio and F.D. Garber, SPIE Proceedings series vol. 5808 (SPIE, Bellingham, WA, 2005), pp. 142-155.

- "Microlocal ISAR for low signal-to-noise environments", M. Cheney and B. Borden, Proceedings of 2006 IEEE Radar conference, Verona, NY.

- Clutter rejecting waveforms for synthetic aperture radar traversing arbitrary flight path", B. Yazici, C.E. Yarman, and M. Cheney, IEEE Waveform Diversity 2006, Hawaii, January 2006.

- "Radar imaging with independently moving transmitters and receivers", M. Cheney and B. Yazici, Defense Applications of Signal Processing, December 10-15, 2006, Fraser Island, Australia.

- "Bistatic synthetic aperture hitchhiker imaging", C.E. Yarman, B. Yazici, M. Cheney, ICASSP 2007.

- "Synthetic Aperture Imaging using Sources of Opportunity", C.E. Yarman, B. Yazici, and M. Cheney, SPIE Defense & Security Conference 2007.

- "Radar detection using sparsely distributed apertures in urban environments", I.-Y. Son, T. Varslot, C.E. Yarman, A. Pezeshki, B. Yazici, and M. Cheney, SPIE Defense & Security Conference 2007

- "Waveform preconditioning for clutter rejection", T. Varslot, B. Yazici, C.E. Yarman, M. Cheney, L. Scharf, SPIE Defense & Security Conference 2007.

- "Identification of multiple-scattering events from 3D GTD-based parametric scattering models", M. Ferrara, M. Cheney, and G. Arnold, SPIE Defense & Security Conference 2007.
- "Two joint time-frequency transforms for velocity separation of moving target radar data", M. Ferrara, G. Arnold, and M. Cheney, SPIE Defense & Security Conference 2007.
- "Radar Imaging", M. Cheney, in proceedings of ICIAM 2007.
- "Imaging that exploits spatial, temporal, and spectral aspects of far-field radar data", M. Cheney and B. Borden, Algorithms for Synthetic Aperture Radar Imagery XV, ed. E.G. Zelnio and F.D. Garber, Proceedings of SPIE Defense & Security Conference, vol. 6970 (2008) 6970 0I doi: 10.1117/12.777416.
- "Waveform Preconditioning for Clutter Rejection in Multipath for Sparse Distributed Apertures, T. Varslot, B. Yazici, C.E. Yarman, M. Cheney, L. Sharf,Proceedings of The Second International Workshop on Computational Advances in Multi-Sensor Adaptive Processing (CAMSAP), pp. 181-184, December 2007.
- "Wideband pulse-echo imaging using distributed apertures in multipath, T. Vaslot, B. Yazici, M. Cheney, SPIE Defense and Security Conference, April, 2008, Orlando, FL.
- "Wideband pulse-echo imaging using distributed apertures in multipath," T. Vaslot, B. Yazici, M. Cheney, IEEE Radar Conference, May, 2008, Rome, Italy.
- Time-reversal Waveform Preconditioning for Clutter Rejection" T. Varslot, B. Yazici, E. Yarman, M. Cheney, L. Scharf, to appear in Applications and Methods of Waveform Diversity, SciTech Publishing, Inc., 2009.

3.2 Dissertations supervised

3.2.1 Matt Ferrara's Thesis

Ph.D. dissertation "Radar Signal Processing", Matt Ferrara, December 2006. Matt Ferrara addressed three problems in his dissertation.

The first problem dealt with binary sequences whose autocorrelations have low sidelobes. Matt used state-of-the-art optimization software to find desirable binary sequences that were previously unknown.

The second and third problems dealt with a group-theoretic method originally developed by Mark Stuff to find the configuration of scattering centers undergoing complex rigid-body rotation. First, Matt found an alternative approach to the time-frequency analysis step. This alternative approach later led to dramatic reductions in the computational time needed for the algorithm.

Next, Matt developed a method for identifying multiple scattering events in the data.

3.2.2 Imaging from sparse measurements

Ph.D. dissertation "Imaging from Sparse Measurements", Yi Fang, December 2008. It is available at
`http://eaton.math.rpi.edu/faculty/Cheney/theses/YiFangThesis.pdf`

This dissertation considers the inverse problem for the scalar wave equation with sparse and non-equally spaced sources and receivers. We develop a method to weight different parts of the data differently to compensate for nonuniform sampling.

We use the single-scattering (Born) approximation and an inversion formula based on a filtered version of the adjoint operator of the forward model. We study the point-spread function to determine the resolution of the reconstruction. For sparsely positioned sources and receivers, the point-spread function can be approximated by a weighted sum of oscillatory functions. A regularized least-squares method can be formulated to determine weights that make the point-spread function as close as possible to the Dirac delta function. Once the weights are determined, the same set of weights can be applied to form an image from measured data.

We test our minimization scheme with different regularization parameters. The sensitivity of the reconstruction with respect to noise and positioning error is tested. We can choose regularization parameters properly to improve resolution and gain stability at the same time.

We show examples of point-spread functions constructed with weights corresponding to three different types of source-receiver geometry with different frequency bands. These results not only show that using the right weights

improves the resolution relative to reconstructions with constant weights, but also illustrate the relation between resolution and the source-receiver geometry and bandwidth.

3.2.3 SAR through a dispersive medium

Ph.D. dissertation "Synthetic-Aperture Radar Imaging and Waveform Design for Dispersive Media", José Héctor Morales Bárcenas, December 2008. It is available at
`http://eaton.math.rpi.edu/faculty/Cheney/theses/HectorMoralesThesis.pdf`

This dissertation develops a method for synthetic-aperture radar (SAR) imaging through a dispersive medium and we provide a method to obtain the optimal waveform design for imaging.

We consider the case when the sensor and scatterers are embedded in a homogeneous dispersive material, and the scene to be imaged lies on a known surface. We use a linearized (Born) scalar scattering model, and allow the flight path of the radar antenna to be an arbitrary smooth curve.

We formulate our filtered back-projection imaging algorithm in a statistical framework where the measurements are polluted with thermal noise. We assume that we have prior knowledge about the power-spectral densities of the scene and the noise.

We test our algorithms when the scene consists of point-like scatterers located on the ground. The position of the targets is well resolved when the target-to-noise ratio is relatively small. For relatively large noise levels, the position of the targets are still well resolved employing the optimal waveform as an input signal in the reconstruction algorithm.

We show the results of simulations in which the dispersive material is modeled with the Fung-Ulaby equations for leafy vegetation. However, the method is also applicable to other dielectric materials where the dispersion is considered relevant in a frequency range of the transmitted signals.

Chapter 4

Current Status of Effort

Work is ongoing to finish up a number of projects.

- Brett Borden and I are working to finish a paper showing how to combine temporal, spatial, and spectral aspects of monostatic SAR data. This paper will probably go to Inverse Problems.
- I am working with my student Yi Fang to finish the paper on his dissertation. This paper is "Imaging from sparse measurements, Y. Fang, M. Cheney, S. Roecker, to be submitted to the Journal of Geophysical Research.
- I am working with Hector Morales and Trond Varslot to finish two papers from Hector's disseration. The first is "Synthetic-aperture imaging through a dispersive medium, T. Varslot, H. Morales, M. Cheney, which we plan to submit to Inverse Problems soon. The second is on waveform design for this problem.
- I worked out a simple model for polarimetric scattering from a dipole. I am working with Katie Voccola, Matt Ferrara, and Birsen Yazıcı to use this to develop an approach for exploiting polarimetric radar data to identify lines and curves in a scene. We periodically update Richard Albanese on our progress.
- Birsen Yazıcı and Ling Wang are working to finish up work motivated by our DARPA project that ended in the spring of 2007. The current manuscript, namely "Radar detection using sparsely distributed

apertures in urban environments", Ling Wang, Il-Young Son, Trond Varslot, C. Evren Yarman, Ali Pezeshki, Birsen Yazici, M. Cheney, and R. Bonneau, is currently being split into two shorter papers. At this time, my involvement on this is only peripheral.

I have also made a start on a number of new projects.

- Brett Borden, Matt Ferrara, and I have plans to combine the work that Brett and I have been doing with tracking ideas.
- I believe I can also use ideas from my joint work with Brett to address the problem of materials identification from SAR data. I have worked out a mathematical model for the data, and have some ideas for how to form an image that contains information about material properties.

Appendix A

Manuscripts Under Review

Multistatic Radar Imaging of Moving Targets

Margaret Cheney, *Member, IEEE,* Brett Borden, and Ling Wang

Abstract

We develop a linearized imaging theory that combines the spatial, temporal, and spectral aspects of scattered waves. We consider the case of fixed sensors and a general distribution of objects, each undergoing linear motion; thus the theory deals with imaging distributions in phase space. We derive a model for the data that is appropriate for narrowband waveforms in the case when the targets are moving slowly relative to the speed of light. From this model, we develop a phase-space imaging formula that can be interpreted in terms of filtered backprojection or matched filtering. For this imaging approach, we derive the corresponding phase-space point-spread function. We show plots of the phase-space point-spread function for various geometries. We also show that in special cases, the theory reduces to: a) Range-Doppler imaging, b) Inverse Synthetic Aperture Radar (ISAR), c) Synthetic Aperture Radar (SAR), d) Doppler SAR, and e) Tomography of Moving Targets. In particular, we note that the theory gives a new SAR-like imaging algorithm for waveforms with arbitrary ridge-like ambiguity functions.

Index Terms

multistatic radar, MIMO radar, ambiguity function

I. Introduction

The well-known techniques of Synthetic-Aperture Radar (SAR) [11], [25], [27] and Inverse Synthetic-Aperture Radar (ISAR) imaging [3], [4] typically use high range-resolution waveforms to measure the range to target scatterers. During the measurement process, the relative locations of target and sensors change in a way that is assumed to be known; these changes in relative position create a "synthetic aperture" that allows an image to be formed by a tomographic process. When the assumptions about the relative motion between target and sensors are incorrect, the

M. Cheney and Ling Wang are with the Department of Mathematical Sciences, Rensselaer Polytechnic Institute, Troy, NY 12180 USA

B. Borden is with the Physics Department, Naval Postgraduate School, Monterey, CA 93943 USA

reconstructed image suffers from unwanted artifacts. For example, most SAR processing assumes that the target scene is stationary, and consequently moving targets are typically either mis-positioned or appear as streaks in the image [10].

For an imaging region containing moving objects, on the other hand, it is well-known that measurements of the Doppler shift can be used to obtain information about velocities. This principle is the foundation of some police radar systems and Moving Target Indicator (MTI) radar systems. Classical "radar ambiguity" theory [28], [9], [16] for monostatic radar shows that measurement accuracy of Doppler shift and time delay depends on the transmitted waveform. There are similar results for the bistatic case in which the transmitter and receiver are at different locations [28], [26], [27]. Some recent work [6] develops a way to combine range and Doppler information measured at multiple receivers in order to maximize the probability of detection.

In recent years there have been a number of attempts to develop imaging techniques that can handle moving objects. Space-Time Adaptive Processing (STAP) [15] uses a moving multiple-element array together with a real-aperture imaging technique to produce Ground Moving Target Indicator (GMTI) image information. Velocity Synthetic Aperture Radar (VSAR) [12] also uses a moving multiple-element array to form a complex-valued SAR image from each element of the array; then, from a comparison of image phases, the system deduces target motion. The approach proposed in [21] uses a separate transmitter and reciever together with sequential pulses to estimate target motion from multiple looks. Another technique [22] uses backscattering data from a single sensor to identify rigid-body target motion, which is then used to form a three-dimensional image. Other work [14], [17] estimates target velocity by finding an along-track relative velocity that causes moving-target streak image artifacts to focus. All of these techniques make use of the so-called "start-stop approximation," in which a target in motion is assumed to be momentarily stationary while it is being interrogated by a radar pulse. In other words, these systems *do not actually measure* the Doppler shift.

Imaging techniques that rely on Doppler data are generally real-aperture systems and provide spatial information with very low resolution. A SAR-like imaging method that uses only Doppler data from a moving sensor and stationary scene was developed in [5]. Another approach [13] uses multiple transmitters and receivers (together with matched-filter processing) to both form an image and estimate the target velocity.

A notional diagram of these theories appears in Fig. 1. It appears that these methods are

special cases of a more general — though, as yet poorly understood — theory that handles all three imaging schemes and which would be located in the center of Fig. 1. Such a theory was proposed in [8]. This work showed how to fuze the spatial, temporal, and spectral aspects of scattered-field-based imaging in the context of fixed distributed sensors and multiple moving targets. The present work more fully develops the special cases that are of interest to radar-based imaging.

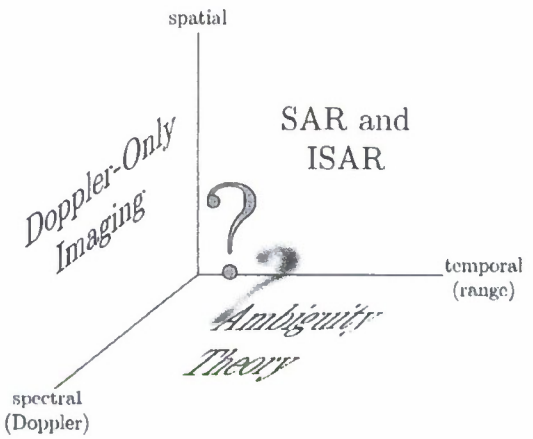

Fig. 1. A diagram of various theories that combine spatial, spectral, and temporal aspects of scattered waves.

In section 2, we develop a physics-based mathematical model that incorporates not only the waveform and wave propagation effects due to moving scatterers, but also the effects of spatial diversity of transmitters and receivers. In section 3, we show how a matched-filtering technique produces images that depend on target velocity, and we relate the resulting point-spread function to the classical radar ambiguity function. We show 4-dimensional plots of the point-spread function for three different geometries. Finally, in section 4, we note that the general theory of section 3 reduces to familiar results, including classical ambiguity theory, ISAR, SAR, and Doppler SAR. We also show that the theory provides a new imaging algorithm for certain waveforms.

II. Model for Data

We model wave propagation and scattering by the scalar wave equation for the wavefield $\psi(t, \boldsymbol{x})$ due to a source waveform $\tilde{s}(t, \boldsymbol{x})$:

$$[\nabla^2 - c^{-2}(t, \boldsymbol{x})\partial_t^2]\psi(t, \boldsymbol{x}) = \tilde{s}(t, \boldsymbol{x})\,. \tag{1}$$

For example, a single isotropic source located at $\boldsymbol{y}$ transmitting the waveform $s(t)$ starting at time $t = -T_{\boldsymbol{y}}$ could be modeled as $\tilde{s}(t, \boldsymbol{x}) = \delta(\boldsymbol{x} - \boldsymbol{y})s_{\boldsymbol{y}}(t + T_{\boldsymbol{y}})$, where the subscript $\boldsymbol{y}$ reminds us that different transmitters could transmit different waveforms. For simplicity, in this discussion we consider only localized isotropic sources; the work can easily be extended to more realistic antenna models [18].

A single scatterer moving at velocity $\boldsymbol{v}$ corresponds to an index-of-refraction distribution $n^2(\boldsymbol{x} - \boldsymbol{v}t)$:

$$c^{-2}(t, \boldsymbol{x}) = c_0^{-2}[1 + n^2(\boldsymbol{x} - \boldsymbol{v}t)]\,, \tag{2}$$

where c_0 denotes the speed of light in vacuum. We write $q_{\boldsymbol{v}}(\boldsymbol{x} - \boldsymbol{v}t) = c_0^{-2}n^2(\boldsymbol{x} - \boldsymbol{v}t)$. To model multiple moving scatterers, we let $q_{\boldsymbol{v}}(\boldsymbol{x} - \boldsymbol{v}t)\,\mathrm{d}^3x\,\mathrm{d}^3v$ be the corresponding quantity for the scatterers in the volume $\mathrm{d}^3x\,\mathrm{d}^3v$ centered at $(\boldsymbol{x}, \boldsymbol{v})$. Thus $q_{\boldsymbol{v}}$ is the distribution, at time $t = 0$, of scatterers moving with velocity $\boldsymbol{v}$. Consequently, the scatterers in the spatial volume d^3x (at $\boldsymbol{x}$) give rise to

$$c^{-2}(t, \boldsymbol{x}) = c_0^{-2} + \int q_{\boldsymbol{v}}(\boldsymbol{x} - \boldsymbol{v}t)\,\mathrm{d}^3v\,. \tag{3}$$

We note that the physical interpretation of $q_{\boldsymbol{v}}$ involves a choice of time origin. The choice that is particularly appropriate, in view of our assumption about linear target velocities, is a time during which the wave is interacting with targets of interest. This implies that the activation of the antenna at $\boldsymbol{y}$ takes place at a negative time which we denote by $-T_{\boldsymbol{y}}$; we write $\tilde{s}(t, \boldsymbol{x}) = s_{\boldsymbol{y}}(t + T_{\boldsymbol{y}})\delta(\boldsymbol{x} - \boldsymbol{y})$. The wave equation corresponding to (3) is then

$$\left[\nabla^2 - c_0^{-2}\partial_t^2 - \int q_{\boldsymbol{v}}(\boldsymbol{x} - \boldsymbol{v}t)\,\mathrm{d}^3v\,\partial_t^2\right]\psi(t, \boldsymbol{x}) = s_{\boldsymbol{y}}(t + T_{\boldsymbol{y}})\delta(\boldsymbol{x} - \boldsymbol{y})\,. \tag{4}$$

In the *absence* of scatterers, the field from the antenna is

$$\psi^{\mathrm{in}}(t, \boldsymbol{x}, \boldsymbol{y}) = -\frac{s_{\boldsymbol{y}}(t + T_{\boldsymbol{y}} - |\boldsymbol{x} - \boldsymbol{y}|/c)}{4\pi|\boldsymbol{x} - \boldsymbol{y}|} \tag{5}$$

We write $\psi = \psi^{\text{in}} + \psi^{\text{sc}}$ and neglect multiple scattering (i.e., use the weak-scatterer model) to obtain the expression for the scattered field ψ^{sc}:

$$\psi^{\text{sc}}(t,\boldsymbol{z}) = \int \frac{\delta(t-t'-|\boldsymbol{z}-\boldsymbol{x}|/c)}{4\pi|\boldsymbol{z}-\boldsymbol{x}|} \int q_{\boldsymbol{v}}(\boldsymbol{x}-\boldsymbol{v}t')\,\mathrm{d}^3v\,\partial_{t'}^2 \frac{s_{\boldsymbol{y}}(t'+T_{\boldsymbol{y}}-|\boldsymbol{x}-\boldsymbol{y}|/c)}{4\pi|\boldsymbol{x}-\boldsymbol{y}|}\,\mathrm{d}^3x\,\mathrm{d}t'. \quad (6)$$

Many radar systems use a *narrowband waveform*, which in our case is defined by

$$s_{\boldsymbol{y}}(t,\boldsymbol{y}) = a_{\boldsymbol{y}}(t,\boldsymbol{y})\,\mathrm{e}^{-\mathrm{i}\omega_{\boldsymbol{y}}t} \quad (7)$$

where $a_{\boldsymbol{y}}(t)$ is *slowly varying*, as a function of t, in comparison with $\exp(-\mathrm{i}\omega_{\boldsymbol{y}}t)$, where $\omega_{\boldsymbol{y}}$ is the carrier frequency for the transmitter at position $\boldsymbol{y}$. For such waveforms, the second time derivative of $s_{\boldsymbol{y}}$ obcys $\ddot{s}_{\boldsymbol{y}}(t) \approx -\omega_{\boldsymbol{y}}^2 s_{\boldsymbol{y}}(t)$.

In equation (6), we make the change of variables $\boldsymbol{x} \mapsto \boldsymbol{x}' = \boldsymbol{x} - \boldsymbol{v}t'$, (i.e., change the frame of reference to one in which the scatterer $q_{\boldsymbol{v}}$ is fixed) to obtain

$$\psi^{\text{sc}}(t,\boldsymbol{z}) = -\int \frac{\delta(t-t'-|\boldsymbol{x}'+\boldsymbol{v}t'-\boldsymbol{z}|/c)}{4\pi|\boldsymbol{x}'+\boldsymbol{v}t'-\boldsymbol{z}|} \int \frac{q_{\boldsymbol{v}}(\boldsymbol{x}')}{4\pi|\boldsymbol{x}'+\boldsymbol{v}t'-\boldsymbol{y}|} \times\ \omega_{\boldsymbol{y}}^2 s_{\boldsymbol{y}}(t'+T_{\boldsymbol{y}}-|\boldsymbol{x}'+\boldsymbol{v}t'-\boldsymbol{y}|/c)\,\mathrm{d}^3x'\,\mathrm{d}^3v\,\mathrm{d}t'. \quad (8)$$

The physical interpretation of (8) is as follows: The wave that emanates from $\boldsymbol{y}$ at time $-T_{\boldsymbol{y}}$ encounters a target at time t'; this target, during the time interval $[0,t']$, has moved from $\boldsymbol{x}$ to $\boldsymbol{x}+\boldsymbol{v}t'$; the wave scatters with strength $q_{\boldsymbol{v}}(\boldsymbol{x})$, and then propagates from position $\boldsymbol{x}+\boldsymbol{v}t'$ to $\boldsymbol{z}$, arriving at time t. Henceforth we will drop the primes on $\boldsymbol{x}$.

Next we assume that the target is slowly moving. More specifically, we assume that $|\boldsymbol{v}|t$ and $k|\boldsymbol{v}|^2t^2$ are much less than $|\boldsymbol{x}-\boldsymbol{z}|$ and $|\boldsymbol{x}-\boldsymbol{y}|$, where $k = \omega_{\max}/c$, with $\omega_{\max}$ the (effective) maximum angular frequency of all the signals $s_{\boldsymbol{y}}$. In this case, expanding $|\boldsymbol{z}-(\boldsymbol{x}+\boldsymbol{v}t)|$ around $t=0$, yields

$$|\boldsymbol{z}-(\boldsymbol{x}+\boldsymbol{v}t)| \approx R_{\boldsymbol{x},\boldsymbol{z}} + \widehat{\boldsymbol{R}}_{\boldsymbol{x},\boldsymbol{z}} \cdot \boldsymbol{v}t \quad (9)$$

where $\boldsymbol{R}_{\boldsymbol{x},\boldsymbol{z}} = \boldsymbol{x}-\boldsymbol{z}$, $R_{\boldsymbol{x},\boldsymbol{z}} = |\boldsymbol{R}_{\boldsymbol{x},\boldsymbol{z}}|$, and $\widehat{\boldsymbol{R}}_{\boldsymbol{x},\boldsymbol{z}} = \boldsymbol{R}_{\boldsymbol{x},\boldsymbol{z}}/R_{\boldsymbol{x},\boldsymbol{z}}$.

We can carry out the t' integration in (8) as follows: we make the change of variables

$$t'' = t - t' - \left(R_{\boldsymbol{x},\boldsymbol{z}} + \widehat{\boldsymbol{R}}_{\boldsymbol{x},\boldsymbol{z}} \cdot \boldsymbol{v}t'\right)/c \quad (10)$$

which has the corresponding Jacobian

$$\left|\frac{\partial t'}{\partial t''}\right| = \frac{1}{|\partial t''/\partial t'|} = \frac{1}{1+\widehat{\boldsymbol{R}}_{\boldsymbol{x},\boldsymbol{z}} \cdot \boldsymbol{v}/c}.$$

We denote the denominator of this Jacobian as $\mu_{z,v}$. The argument of the delta function in (8) contributes only when $t'' = 0$; using (10), this can which can be solved for t' to yield

$$t' = \frac{t - R_{x,z}/c}{1 + \widehat{\boldsymbol{R}}_{x,z} \cdot \boldsymbol{v}/c} \tag{11}$$

The argument of s in equation (8) is then

$$\begin{aligned} t' + T_y - \frac{|\boldsymbol{x} + \boldsymbol{v}t' - \boldsymbol{y}|}{c} &\approx t' + T_y - \left(\frac{R_{x,y}}{c} + \frac{\widehat{\boldsymbol{R}}_{x,y} \cdot \boldsymbol{v}}{c} t' \right) \\ &= \frac{1 - \widehat{\boldsymbol{R}}_{x,y} \cdot \boldsymbol{v}/c}{1 + \widehat{\boldsymbol{R}}_{x,z} \cdot \boldsymbol{v}/c} \left(t - \frac{R_{x,z}}{c} \right) - \frac{R_{x,y}}{c} + T_y \end{aligned} \tag{12}$$

where we have used (9) and (11). The quantity

$$\alpha_{x,v} = \frac{1 - \widehat{\boldsymbol{R}}_{x,y} \cdot \boldsymbol{v}/c}{1 + \widehat{\boldsymbol{R}}_{x,z} \cdot \boldsymbol{v}/c} \approx 1 - (\widehat{\boldsymbol{R}}_{x,y} + \widehat{\boldsymbol{R}}_{x,z}) \cdot \boldsymbol{v}/c \tag{13}$$

is the *Doppler scale factor*. If we write the Doppler scale factor (13) as $\alpha_{x,v} \approx 1 + \beta_{x,v}$, where

$$\beta_{x,v} = -(\widehat{\boldsymbol{R}}_{x,y} + \widehat{\boldsymbol{R}}_{x,z}) \cdot \boldsymbol{v}/c \tag{14}$$

then the quantity $\omega_y \beta_{x,v}$ is the (angular) *Doppler shift*. We note that the Doppler shift depends on the bistatic bisector vector $\widehat{\boldsymbol{R}}_{x,y} + \widehat{\boldsymbol{R}}_{x,z}$ (see Fig. 2).

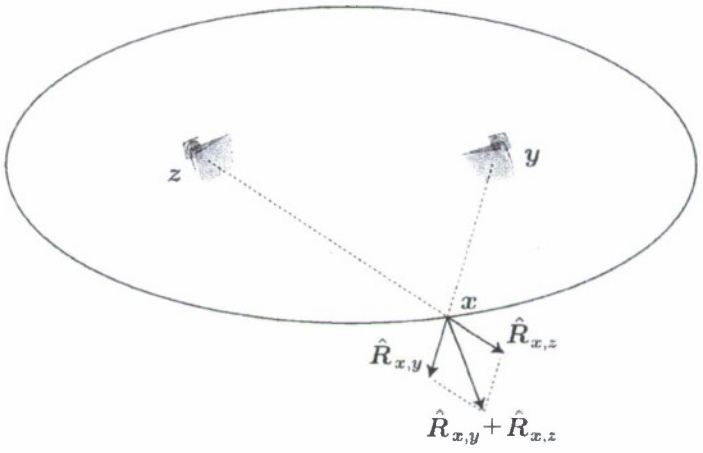

Fig. 2. The bistatic range is the sum of the distances $R_{x,z}$ and $R_{x,y}$, and the bistatic bisector is the vector $\widehat{\boldsymbol{R}}_{x,y} + \widehat{\boldsymbol{R}}_{x,z}$.

With (12) and thc notation of equation (13), equation (8) becomes

$$\psi^{\mathrm{sc}}(t, \boldsymbol{z}, \boldsymbol{y}) = -\omega_y^2 \int \frac{s_y \left[\alpha_{x,v} (t - R_{x,z}/c) - R_{x,y}/c + T_y \right]}{(4\pi)^2 R_{x,z} R_{x,y} \mu_{z,v}} q_v(\boldsymbol{x}) \, \mathrm{d}^3 x \, \mathrm{d}^3 v \tag{15}$$

We use (7) to write

$$s_y\left[\alpha_{x,v}\left(t - R_{x,z}/c\right) - R_{x,y}/c + T_y\right] \approx a_y[t - R_{x,z}/c - R_{x,y}/c + T_y] \\ \mathrm{e}^{-\mathrm{i}\omega_y[(1+\beta_{x,v})(t-R_{x,z}/c)-R_{x,y}/c+T_y]} \tag{16}$$

where we have used the fact that a_y is slowly varying to replace $\alpha_{x,v}$ by 1. With equation (16), equation (15) becomes

$$\psi^{\mathrm{sc}}(t, \boldsymbol{z}, \boldsymbol{y}) \approx -\int \frac{\omega_y^2\, \mathrm{e}^{\mathrm{i}\varphi_{x,v}}\, \mathrm{e}^{-\mathrm{i}\omega_y \alpha_{x,v} t}}{(4\pi)^2 R_{x,z} R_{x,y} \mu_{z,v}} a_y\left(t + T_y - (R_{x,z} + R_{x,y})/c\right) q_v(\boldsymbol{x})\, \mathrm{d}^3x\, \mathrm{d}^3v \tag{17}$$

Here we have collected the time-independent terms in the exponent into the quantity

$$\varphi_{x,v} = k_y\left[R_{x,y} - T_y + \tilde{\alpha}_{x,v} R_{x,z}\right], \tag{18}$$

where $k_y = \omega_y/c$.

We recognize (17) as the familiar superposition of time-delayed and Doppler-shifted copies of the transmitted waveform.

III. Imaging

We now address the question of extracting information from the scattered waveform described by equation (15).

Our image formation algorithm depends on the data we have available. In general, we will form a (coherent) image as a filtered adjoint [18], but the variables we integrate over depend on whether we have multiple transmitters, multiple receivers, and/or multiple frequencies. The *number* of variables we integrate over, in turn, determines how many image dimensions we can hope to reconstruct. If our data depend on two variables, for example, then we can hope to reconstruct a two-dimensional scene; in this case the scene is commonly assumed to lie on a known surface. If, in addition, we want to reconstruct two-dimensional velocities, then we are seeking a four-dimensional image and thus we will require data depending on at least four variables. More generally, the problem of determining a distribution of positions in space and the corresponding three-dimensional velocities means that we seek to form an image in a six-dimensional phase space.

A. Imaging Formula

We form an image $I_{\boldsymbol{u}}(\boldsymbol{p})$ of the objects with velocity $\boldsymbol{u}$ that, at time $t = 0$, were located at position $\boldsymbol{p}$. Thus $I_{\boldsymbol{u}}(\boldsymbol{p})$ is constructed to be an approximation to $q_{\boldsymbol{u}}(\boldsymbol{p})$.

We form an image by matched filtering:

$$I_{\boldsymbol{u}}(\boldsymbol{p}) = (4\pi)^2 \int \mathrm{e}^{-\mathrm{i}\varphi_{\boldsymbol{p},\boldsymbol{u}}} \mathrm{e}^{\mathrm{i}\omega_{\boldsymbol{y}}\alpha_{\boldsymbol{p},\boldsymbol{u}}t} R_{\boldsymbol{p},\boldsymbol{z}} R_{\boldsymbol{p},\boldsymbol{y}} \mu_{\boldsymbol{z},\boldsymbol{u}} \times a_{\boldsymbol{y}}^*\left(t + T_{\boldsymbol{y}} - (R_{\boldsymbol{p},\boldsymbol{z}} + R_{\boldsymbol{p},\boldsymbol{y}})/c\right) \psi^{\mathrm{sc}}(t, \boldsymbol{z}, \boldsymbol{y}) J \,\mathrm{d}t \,\mathrm{d}^n z \,\mathrm{d}^m y \tag{19}$$

where J is a geometry-dependent weighting function that can be inserted to improve the image [18]. Here we take $n = 1, 2$ or 3, depending on the receiver configuration, and $m = 1, 2$, or 3, depending on the transmitter configuration. For a limited number of discrete receivers (or transmitters), the integral over $\boldsymbol{z}$ (or $\boldsymbol{y}$) in (19) reduces to a sum.

In allowing the imaging operation (19) to depend on the transmitter $\boldsymbol{y}$, we are implicitly assuming that, at the receiver located at $\boldsymbol{z}$, we can identify the part of the signal $\psi^{sc}(t, \boldsymbol{z}, \boldsymbol{y})$ that is due to the transmitter at $\boldsymbol{y}$. In the case of multiple transmitters, this identification can be accomplished, for example, by having different transmitters operate at different frequencies or, possibly, by quasi-orthogonal pulse-coding schemes. We are also assuming a coherent system, i.e., that a common time clock is available to all sensors.

The operation (19) amounts to geometry-corrected and phase-corrected matched filtering with a time-delayed, Doppler-shifted version of the transmitted waveform, where the Doppler shift is defined in terms of (14).

B. Image Analysis

We substitute equation (17) into equation (19), obtaining

$$I_{\boldsymbol{u}}(\boldsymbol{p}) = \int K(\boldsymbol{p}, \boldsymbol{u}; \boldsymbol{x}, \boldsymbol{v})\, q_{\boldsymbol{v}}(\boldsymbol{x}) \,\mathrm{d}^3 x \,\mathrm{d}^3 v \tag{20}$$

where K, the point-spread function (PSF) is

$$K(\boldsymbol{p}, \boldsymbol{u}; \boldsymbol{x}, \boldsymbol{v}) = -\int \omega_{\boldsymbol{y}}^2 a_{\boldsymbol{y}}^*\left(t + T_{\boldsymbol{y}} - (R_{\boldsymbol{p},\boldsymbol{z}} + R_{\boldsymbol{p},\boldsymbol{y}})/c\right) \mathrm{e}^{\mathrm{i}\omega_{\boldsymbol{y}}[\beta_{\boldsymbol{p},\boldsymbol{u}} - \beta_{\boldsymbol{x},\boldsymbol{v}}]t} \times a_{\boldsymbol{y}}\left(t + T_{\boldsymbol{y}} - (R_{\boldsymbol{x},\boldsymbol{z}} + R_{\boldsymbol{x},\boldsymbol{y}})/c\right) \exp\left(\mathrm{i}[\varphi_{\boldsymbol{x},\boldsymbol{v}} - \varphi_{\boldsymbol{p},\boldsymbol{u}}]\right) \times \frac{R_{\boldsymbol{p},\boldsymbol{z}} R_{\boldsymbol{p},\boldsymbol{y}} \mu_{\boldsymbol{z},\boldsymbol{u}}}{R_{\boldsymbol{x},\boldsymbol{z}} R_{\boldsymbol{x},\boldsymbol{y}} \mu_{\boldsymbol{z},\boldsymbol{v}}} J \,\mathrm{d}t \,\mathrm{d}^n z \,\mathrm{d}^m y \tag{21}$$

In the second exponential of equation (21) we use (18) to write

$$\begin{aligned}\varphi_{x,v} - \varphi_{p,u} &= k_y \left[R_{x,y} - T_y + (1+\beta_{x,v})R_{x,z}\right] \\ &\quad - k_y \left[R_{p,y} - T_y + (1+\beta_{p,u})R_{p,z}\right]] \\ &= k_y \Big[- c\Delta\tau_{y,z} + \beta_{x,v}R_{x,z} - \beta_{p,u}R_{p,z}\Big] \end{aligned} \tag{22}$$

where

$$c\Delta\tau_{y,z} = [R_{p,z} + R_{p,y}] - [R_{x,z} + R_{x,y}]. \tag{23}$$

is the difference in bistatic ranges for the points x and p. If in (21) we make the change of variables $t' = t + T_y - (R_{x,z} + R_{x,y})/c$ and use (25), then we obtain

$$\boxed{\begin{aligned} K(\boldsymbol{p},\boldsymbol{u};\boldsymbol{x},\boldsymbol{v}) = -\int \omega_y^2 A_y\left(\omega_y[\beta_{p,u} - \beta_{x,v}], \Delta\tau_{y,z}\right) \exp\left(\mathrm{i}\omega_y[\beta_{p,u} - \beta_{x,v}][R_{x,y}/c - T_y]\right) \\ \times \exp\left(-\mathrm{i}k_y\beta_{p,u}[R_{x,z} - R_{p,z}]\right) \frac{R_{p,z}R_{p,y}\mu_{z,u}}{R_{x,z}R_{x,y}\mu_{z,v}} J\,\mathrm{d}^n z\,\mathrm{d}^m y \end{aligned}} \tag{24}$$

where

$$A_y(\tilde{\omega},\tau) = \mathrm{e}^{-\mathrm{i}\omega_y\tau} \int a_y^*(t-\tau)\, a_y(t)\, \mathrm{e}^{\mathrm{i}\tilde{\omega}t}\,\mathrm{d}t\,. \tag{25}$$

is the *radar ambiguity function*. Equation (24) says the following.

> The multistatic phase-space point-spread function is a weighted coherent sum of radar ambiguity functions evaluated at appropriate bistatic ranges and bistatic velocities.

We note that the bistatic ambiguity function of (24) depends on the difference of bistatic ranges (23) and on the difference between the velocity projections onto the bistatic bisectors $\beta_{p,u} - \beta_{x,v} = (\widehat{\boldsymbol{R}}_{x,y} + \widehat{\boldsymbol{R}}_{x,z}) \cdot \boldsymbol{v}/c - (\widehat{\boldsymbol{R}}_{p,y} + \widehat{\boldsymbol{R}}_{p,z}) \cdot \boldsymbol{u}/c$.

For the case of a single transmitter and single receiver (a case for which $J = 1$) and a point target [which enables us to choose T_y so that the exponential in the top line of (24) vanishes], and leaving aside the magnitude and phase corrections, equation (24) reduces to a coordinate-independent version of the ambiguity function of [24].

C. Examples of the Point-Spread Function

The point-spread function contains all the information about the performance of the imaging system. Unfortunately it is difficult to visualize this PSF because it depends on so many variables. In the case when the positions and velocities are restricted to a known plane, the PSF is a function of four variables.

We would like to know whether we can find both the position and velocity of moving targets. Ideally, the point-spread function is delta-like, and so we can obtain both position and velocity. If, however, the PSF is ridge-like, then there will be uncertainty in some directions or in some combination of positions and velocities.

In order to look for possible ridge-like behavior, we write the PSF as

$$K(\boldsymbol{p}, \boldsymbol{u}; \boldsymbol{x}, \boldsymbol{v}) = K(r(\cos\theta, \sin\theta), s(\cos\phi, \sin\phi), \boldsymbol{x}, \boldsymbol{v}). \tag{26}$$

We plot the PSF for a fixed target position $\boldsymbol{x}$ and target velocity $\boldsymbol{v}$. We then sample θ and ϕ at intervals of $\pi/4$, and for each choice of θ and ϕ, we plot r versus s. This process results in $9 \times 9 = 81$ plots of r versus s. Finally, to show the entire four-dimensional space at a glance, we display all the 81 plots simultaneously on a grid, arranged as shown in Fig. 3.

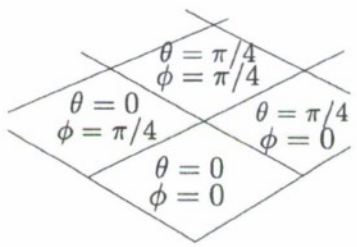

Fig. 3. This shows how Figures 4 - 6 display the four-dimensional point-spread function (26).

1) Simulation Parameters: Our strategy in the simulations is to use a delta-like ambiguity function, and investigate the effect of geometry on the overall point-spread function. In all cases, we use a transmit time of $T_{\boldsymbol{v}} = 0$.

a) Waveform: In the simulations, we use a high-Doppler-resolution, linearly-frequency-modulated (LFM) pulse train. The ambiguity function of this pulse train has a "bed-of-nails" appearance [16], with a delta-like central peak that has good velocity resolution and coarse range resolution. We assume that the extraneous peaks of the ambiguity function occur in a region of space and velocity where no targets are present.

In our simulations, we choose the duration of each pulse to be $T_p = 10 \times 10^{-6}$ s, the pulse period to be $T_R = 10^{-4}$ s, and take $N = 50$ pulses in the pulse train so that the duration of the entire pulse train is $T = NT_R = 5 \times 10^{-3}$ s. The bandwidth B of the pulse train is chosen to

be $B = 3 \times 10^6$Hz. The FM rate is B/T_p. We take the center frequency to be 30GHz, which corresponds to a wavelength of $\lambda = 0.01$m.

The ambiguity function of this pulse train has the following properties.

- The Doppler resolution is $1/T = 200$ s^{-1}, which in the ordinary monostatic case would correspond to down-range velocity resolution of $\Delta V = \lambda/(2T) = 1$ m/s.
- The first ambiguous Doppler value is $1/T_R = 10^4$ s^{-1}, which would correspond to a monostatic velocity ambiguity of $\Delta V_{\max} = \lambda/(2T_R) = 50$ m/s.
- The delay resolution is $1/B \approx .3 \times 10^{-6}$ s, which would correspond to a monostatic range resolution of $\Delta r = c/(2B) = 50$ m.
- The first ambiguous delay is $T_R = 10^{-4}$ s, which corresponds to an ambiguous (monostatic) range of $\Delta r_{\max} = cT_R/2 = 1.5 \times 10^4$ m. This would be the maximum measurable unique range.

b) Area of Interest: The area of interest is a circular region with radius of 1000 m; points within this region differ by no more than 2000m, which is well within the unambiguous range of 15000 m. We assume that there are no scatterers outside the region of interest. The location of every point in the region is denoted by the vector $\boldsymbol{p} = r(\cos\theta, \sin\theta)$. The directions θ are sampled at intervals of $\pi/4$, while the lengths r are sampled at intervals of 25 m.

c) Velocities of Interest: The velocities are written $\boldsymbol{u} = s(\cos\phi, \sin\phi)$. We consider velocity magnitudes in the interval $[0, 30]$ m/s. The magnitudes s are sampled at intervals of 0.5 m/sec and the directions ϕ are sampled at intervals of $\pi/4$.

2) Examples:

a) Single transmitter, two receivers: The point-spread function for a single transmitter and two receivers is shown in Figure 4. Here the transmitter is located at $\boldsymbol{y} = (0, -10000)$ m, the receivers are located at $\boldsymbol{z}_1 = (10000, 0)$ m and $\boldsymbol{z}_2 = (-10000, 0)$ m, the scene of interest is a disk centered at the origin with radius 1000 m, the target location is $225(\cos 45°, \sin 45°)$ m and the target velocity is $20(\cos 0, \sin 0)$ m/s.

We see that for this geometry, the point-spread function is indeed ridge-like.

b) Circular geometry: Figure 5 shows the point-spread function for a circular arrangement of 8 transmitters and 10 receivers. The transmitters are equally spaced around a circle of radius 10000 m; the receivers are equally spaced around a circle of radius 9000 m. The scene of interest has radius 1000 m. The true target location is $225(\cos 180°, \sin 180°)$ m and the true velocity is

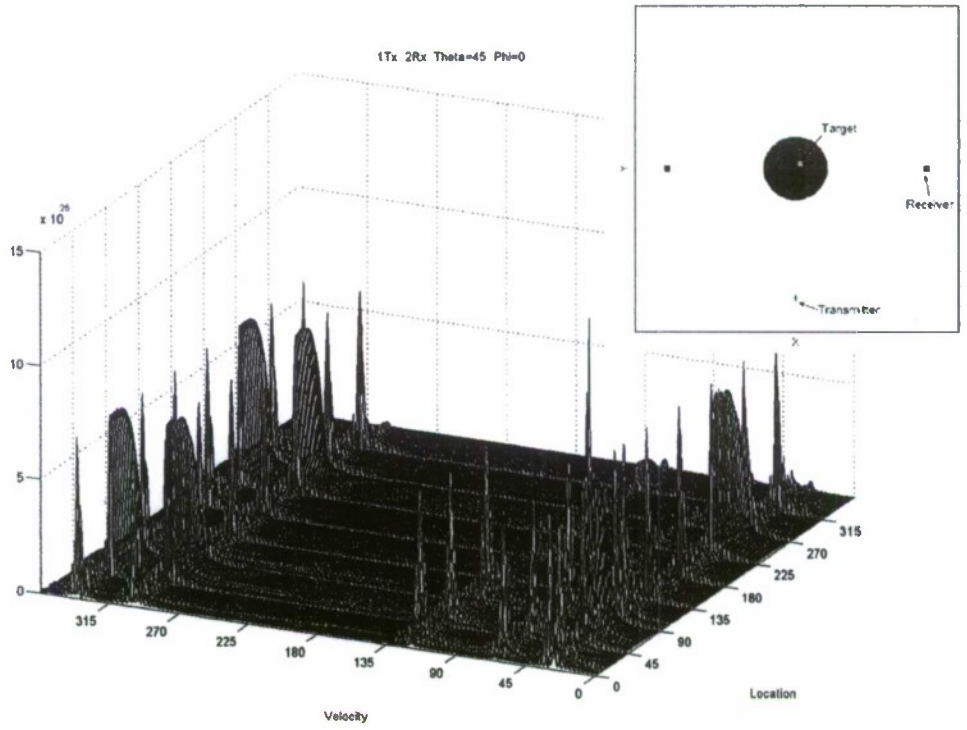

Fig. 4. This shows the geometry (not to scale) for one transmitter and two receivers, together with the the combined point-spread function.

$20(\cos 180°, \sin 180°)$ m/s. For this geometry, there appear to be no ambiguities.

c) Linear array: Figure 6 shows the point-spread function for a linear array of 11 transmitters and a single receiver. In this case, the transmitters are equally spaced along the line $-5000\text{m} \leq x \leq 5000\text{m}, y = 10000\text{m}$; the receiver is located at $(0, 10000)$m; the true target location is $225(\cos 135°, \sin 135°)$ m and the target velocity is $20(\cos 45°, \sin 45°)$ m/s.

IV. Reduction to Familiar Special Cases

The formula (24) reduces correctly to a variety of special cases. More details can be found in [8].

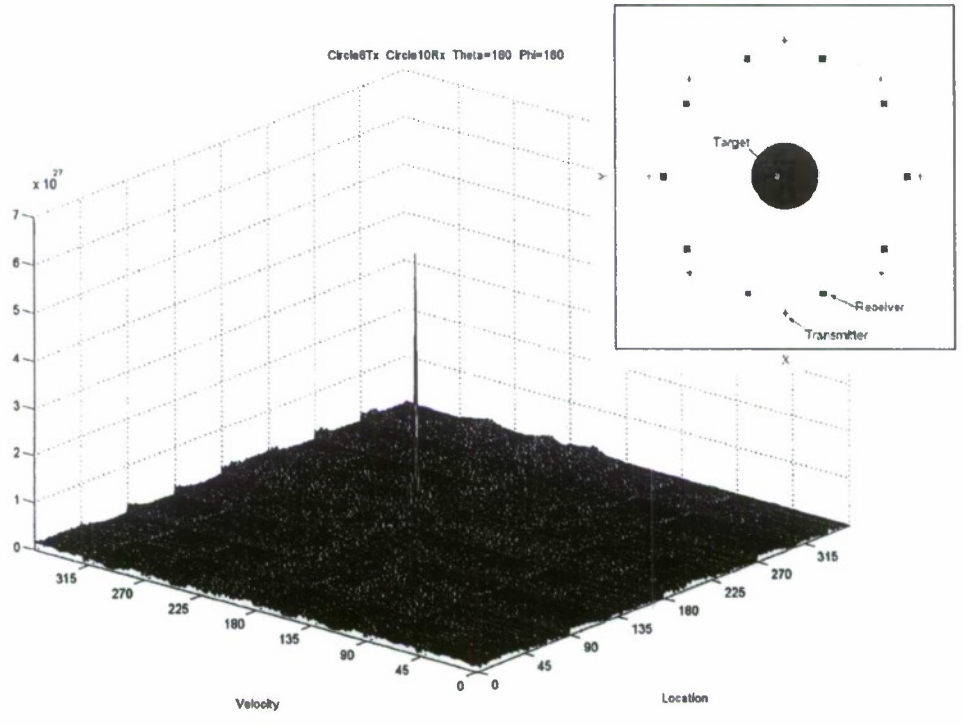

Fig. 5. This shows the geometry (not to scale) for 8 transmitters and 10 receivers arranged in a circle and the corresponding combined point-spread function.

A. *Range-Doppler Imaging*

In classical range-Doppler imaging, the range and velocity of a moving target are estimated from measurements made by a single transmitter and coincident receiver. Thus we take $\boldsymbol{z} = \boldsymbol{y}$, $J = 1$, and remove the integrals in (24) to show that the point-spread function is simply proportional to the classical ambiguity function.

1) Range-Doppler Imaging of a Rotating Target: If the target is rotating about a point, then we can use the connection between position and velocity to form a range-Doppler target image. For the case of turntable geometry, where for a point $(x_1, x_2, 0)$, the range is x_1 and the down-range velocity is $\omega_0 \dot{\theta} x_2$, with ω_0 the center frequency and $\dot{\theta}$ the target rotation rate, (24) reduces

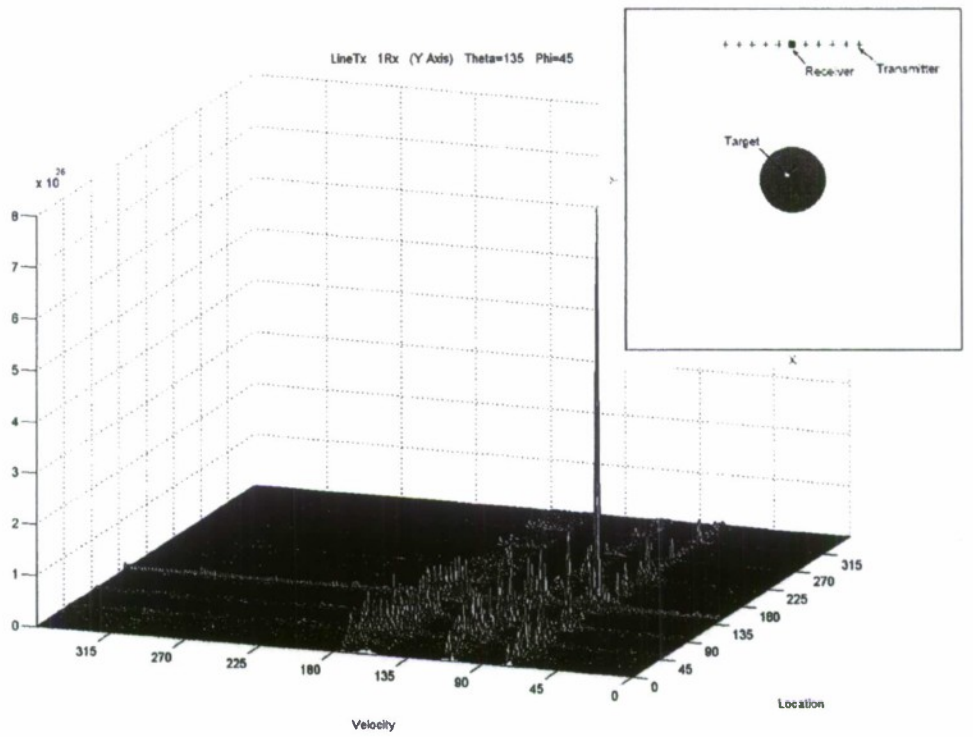

Fig. 6. This shows the geometry (not to scale) for a linear array 11 transmitters and a single receiver and the corresponding combined point-spread function.

to the classical

$$K_{\mathrm{RD}}(\boldsymbol{p},\boldsymbol{u};\boldsymbol{x},\boldsymbol{v}) \propto A_{\boldsymbol{y}}\Big(2\frac{\omega_c\dot{\theta}(p_2-x_2)}{c}, 2\frac{(p_1-x_1)}{c}\Big). \tag{27}$$

B. Inverse Synthetic-Aperture Radar (ISAR)

ISAR systems rely on the target's rotational motion to establish a pseudo-array of distributed receivers, from which range measurements are made. To show how ISAR follows from the results of this paper, we fix the coordinate system to the rotating target. Succeeding pulses of a pulse train are transmitted from and received at positions $\boldsymbol{z} = \boldsymbol{y}$ that rotate around the target as $\hat{\boldsymbol{y}} = \hat{\boldsymbol{y}}(\theta)$. The pulses typically used in ISAR are high range-resolution (HRR) ones, so that each pulse yields a ridge-like ambiguity function $A_{\boldsymbol{y}}(\nu,\tau) = \overline{A}_{\boldsymbol{y}}(\tau)$, with $\overline{A}_{\boldsymbol{y}}(\tau)$ sharply peaked

around $\tau = 0$. Using this ambiguity function in (24) shows that the imaging process corresponds to backprojection [8].

C. Synthetic-Aperture Radar (SAR)

SAR also uses high range-resolution pulses, transmitted and received at locations along the flight path $\boldsymbol{y} = \boldsymbol{y}(\zeta)$, where ζ denotes the flight path parameter. For a stationary scene, $\boldsymbol{u} = \boldsymbol{v} = \mathbf{0}$, which implies that $\beta_{\boldsymbol{u}} = \beta_{\boldsymbol{v}} = 0$. In this case, (24) corresponds to backprojection over circles [19].

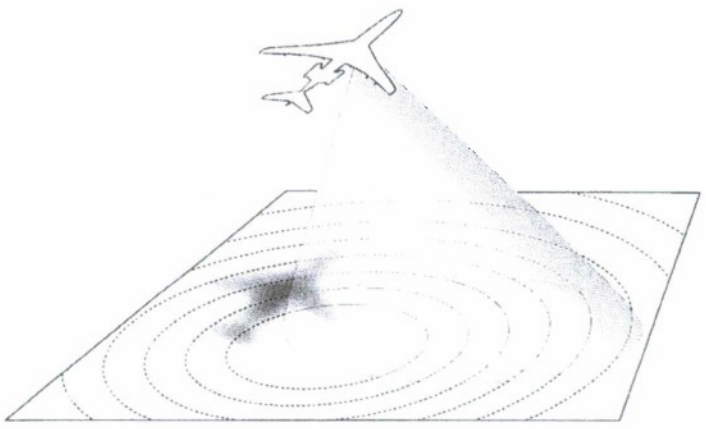

Fig. 7. For SAR, we consider a stationary scene and a sensor that (in the start-stop approximation) does not move as it transmits and receives each pulse. Between pulses, the sensor moves to a different location along the flight path.

D. Doppler SAR

Doppler SAR uses a high Doppler-resolution waveform, such as an approximation to the ideal single-frequency waveform $s(t) = \exp(-\mathrm{i}\omega_0 t)$ transmitted from locations along the flight path $\boldsymbol{y} = \boldsymbol{y}(\zeta)$. If we transform to the sensor frame of reference, then the entire scene is moving with velocity $\boldsymbol{u} = \boldsymbol{v} = -\dot{\boldsymbol{y}}(\zeta)$ (see Fig. 8).

For a high Doppler-resolution waveform, $A_{\boldsymbol{y}}(\nu, \tau) = \overline{A}_{\boldsymbol{y}}(\nu)$, where $\overline{A}_{\boldsymbol{y}}(\nu)$ is sharply peaked around $\nu = 0$. Using this waveform in (24) shows that the imaging process corresponds to backprojection over hyperbolas, as detailed in [5].

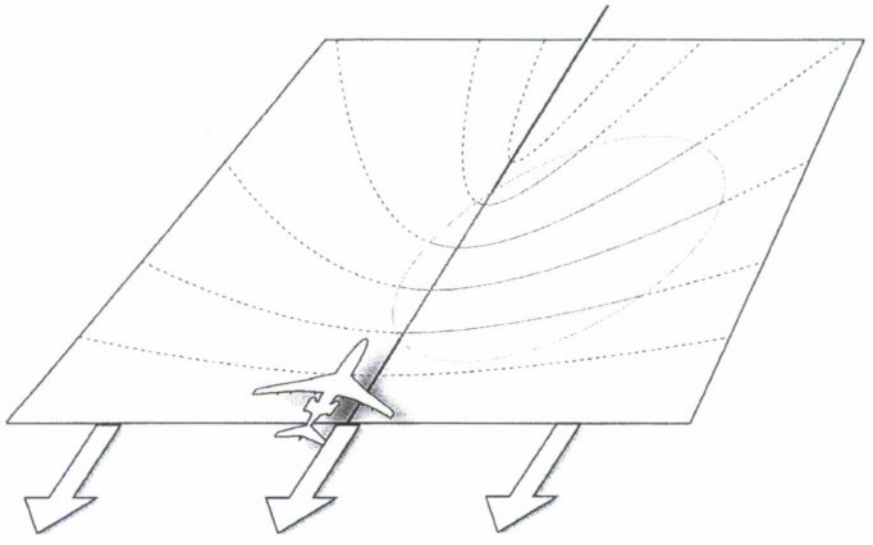

Fig. 8. For Doppler SAR, we use a frame of reference in which the sensor is fixed and the plane below is moving with a uniform velocity.

E. SAR for Other Ridge-like Ambiguity Functions

In the above scenario, SAR reconstruction can be performed with a sensor moving along the path $\boldsymbol{y} = \boldsymbol{y}(\zeta)$ while transmitting other waveforms. In particular, waveforms (such as chirps) can be used which produce a ridge-like ambiguity function along any line $\nu = \eta\tau$ in the delay-Doppler plane [16]. Then (24) corresponds to backprojection over the planar curves $L_{\boldsymbol{p}}(\zeta)$:

$$L_{\boldsymbol{p}}(\zeta) = -\omega_0 \widehat{\boldsymbol{R}}_{\boldsymbol{p},\boldsymbol{y}(\zeta)} \cdot \dot{\boldsymbol{y}}(\zeta) + \eta R_{\boldsymbol{p},\boldsymbol{y}(\zeta)} \tag{28}$$

The curve $L_{\boldsymbol{p}}(\zeta)$ is the intersection of the imaging plane with a surface generated by rotating a limaçon of Pascal (see Fig. 9) about the flight velocity vector. We note that for a slowly-moving sensor and a side-looking beam pattern, the curve obtained from the limaçon is almost indistinguishable from a circle.

F. Moving Target Tomography.

Moving Target Tomography has been proposed in the paper [13], which models the signal using a simplified version of (17). For this simplified model, our imaging formula (19) reduces

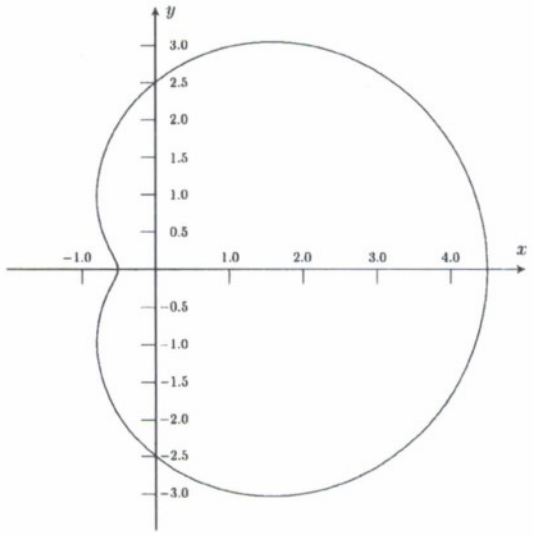

Fig. 9. A limaçon of Pascal. The origin is located at the transmitter position y.

to the approach advocated in [13] — namely matched-filter processing with a different filter for each location p and for each possible velocity u.

V. Conclusions and Future Work

We have developed a linearized imaging theory that combines the spatial, temporal, and spectral aspects of scattered waves.

This imaging theory is based on the general (linearized) expression we derived for waves scattered from moving objects, which we model in terms of a distribution in phase space. The expression for the scattered waves is of the form of a Fourier integral operator; consequently we form a phase-space image as a filtered adjoint of this operator.

The theory allows for activation of multiple transmitters at different times, but the theory is simpler when they are all activated so that the waves arrive at the target at roughly the same time.

The general theory in this paper reduces to familiar results in a variety of special cases. We leave for the future further analysis of the point-spread function. We also leave for the future the case in which the sensors are moving independently, and the problem of combining these ideas with tracking techniques.

VI. ACKNOWLEDGEMENTS

This work was supported by the Office of Naval Research, by the Air Force Office of Scientific Research[1] under agreement number FA9550-06-1-0017, by Rensselaer Polytechnic Institute, and by the National Research Council.

REFERENCES

[1] N. Bleistein, J.K. Cohen, and J.W. Stockwell, *The Mathematics of Multidimensional Seismic Inversion*, (Springer: New York, 2000)

[2] N. Bleistein and R.A. Handelsman, Asymptotic Expansions of Integrals, Dover, New York, 1986.

[3] B. Borden *Radar imaging of Airborne Targets* (Bristol: Institute of Physics, 1999).

[4] B. Borden "Mathematical problems in radar inverse scattering", *Inverse Problems* 18 (2002) R1–R28.

[5] B. Borden and M. Cheney, "Synthetic-Aperture Imaging from High-Doppler-Resolution Measurements," *Inverse Problems*, **21**, pp. 1–11 (2005)

[6] I. Bradaric, G.T. Capraro, D.D. Weiner, and M.C. Wicks, "Multistatic Radar Systems Signal Processing", Proceedings of IEEE Radar Conference 2006.

[7] J. Cooper, "Scattering of Electromagnetic Fields by a Moving Boundary: The One-Dimensional Case", IEEE Antennas and Propagation, vol. AP-28, No. 6, pp. 791–795 (1980).

[8] M. Cheney and B. Borden, "Imaging moving targets from scattered waves," *Inverse Problems*, **24** (2008) 035005.

[9] C.E. Cook and M. Bernfeld, *Radar Signals* (Academic: New York, 1967)

[10] J.R. Fienup, "Detecting moving targets in SAR imagery by focusing", *IEEE Trans. Aero. Electr. Systems* 37 (July 2001) 794–809.

[11] G. Franceschetti and R. Lanari, *Synthetic Aperture Radar Processing*, CRC Press, New York, 1999.

[12] B. Friedlander and B. Porat, "VSAR: A High Resolution Radar System for Detection of Moving Targets," IEE Proc. Radar, Sonar, Navig., **144**, pp. 205–18 (1997)

[13] B. Himed, H. Bascom, J. Clancy, and M.C. Wicks, "Tomography of Moving Targets (TMT)", in *Sensors, Systems, and Next-Generation Satellites V.*, ed. H. Fujisada, J.B. Lurie, and K. Weber, Proc. SPIE Vol. 4540 (2001) pp. 608 – 619.

[14] J.K. Jao, "Theory of Synthetic Aperture Radar Imaging of a Moving Target", *IEEE Trans. Geoscience and Remote Sensing* 39 (September 2001) 1984 – 1992.

[15] R. Klemm, *Principles of Space-Time Adaptive Processing*, (Institution of Electrical Engineers: London, 2002)

[16] N. Levanon, *Radar Principles*, (Wiley, New York, 1988)

[17] M.J. Minardi, L.A. Gorham, and E.G. Zelnio, "Ground Moving Target Detection and Tracking Based on Generaized SAR Processing and Change Detection," Proceedings of SPIE, **5808**, pp. 156–165 (2005)

[18] C.J. Nolan and M. Cheney, "Synthetic Aperture Inversion," Inverse Problems, **18**, pp. 221–36 (2002)

[1]Consequently the U.S. Government is authorized to reproduce and distribute reprints for Governmental purposes notwithstanding any copyright notation thereon. The views and conclusions contained herein are those of the authors and should not be interpreted as necessarily representing the official policies or endorsements, either expressed or implied, of the Air Force Research Laboratory or the U.S. Government.

[19] C.J. Nolan and M. Cheney, "Synthetic Aperture Inversion for Arbitrary Flight Paths and Non-Flat Topography," IEEE Trans. on Image Processing, **12**, pp. 1035–43 (2003)

[20] M. Reed and B. Simon, *Methods of Modern Mathematical Physics. I. Functional Analysis* (Academic Press: New York, 1972)

[21] M. Soumekh, "Bistatic Synthetic Aperture Radar Inversion with Application in Dynamic Object Imaging", IEEE Trans. Signal Processing, Vol. 39, No. 9, pp. 2044–2055 (1991).

[22] M. Stuff, M. Biancalana, G. Arnold, and J. Garbarino, "Imaging Moving Objects in 3D From Single Aperture Synthetic Aperture Data," Proceedings of IEEE Radar Conference 2004, pp. 94–98

[23] D. Swick, "A Review of Wideband Ambiguity Functions," Naval Research Laboratory Rep. 6994 (1969)

[24] T. Tsao, M. Slamani, P. Varshney, D. Weiner, H. Schwarzlander, and S. Borek, "Ambiguity Function for a Bistatic Radar," IEEE Trans. Aerospace & Electronic Systems, **33**, pp. 1041–51 (1997)

[25] N.J. Willis, *Bistatic Radar* (Artech House: Norwood, MA, 1991)

[26] N.J. Willis and H.D. Griffiths, *Advances in Bistatic Radar* (SciTech Publishing, Raleigh, North Carolina, 2007)

[27] N.J. Willis, "Bistatic Radar," in *Radar Handbook*, M. Skolnik, ed., (McGraw-Hill: New York, 1990)

[28] P.M. Woodward, *Probability and Information Theory, with Applications to Radar*, (McGraw-Hill: New York, 1953)

[29] B. Yazici, M. Cheney, and C.E. Yarman, "Synthetic-aperture inversion in the presence of noise and clutter", Inverse Problems **22**, pp. 1705-1729 (2006) .

Time-reversal Waveform Preconditioning for Clutter Rejection using Distributed Apertures in Multi-path Environment

T. Varslot, *Member, IEEE*, B. Yazıcı, *Senior Member, IEEE*, M. Cheney, *Member, IEEE*

Abstract—**We present a time-reversal implementation of a transmit waveform *preconditioning* scheme for optimal clutter rejection in radar imaging. Waveform preconditioning involves determining a map on the space of transmit waveforms, and then applying this map to the waveforms before transmission. We consider a distributed aperture where the antenna elements are distributed spatially in an arbitrary fashion, possibly several hundred wavelengths apart, transmitting from multiple elements simultaneously. We use a physics-based multi-path scattering model for the propagation environment. We design a preconditioning operator using the model for the multi-path scattering environment and a priori target and clutter statistics. We show that, by our time-reversal implementation, we avoid the need for an explicit model for the multi-path environment and a priori target and clutter statistics in order to compute the preconditioning operator. While our focus has been on radar imaging, our work is also applicable to other pulse-echo applications, such as ultrasound, sonar and microwave imaging.**

I. Introduction

In radar applications, the scene (everything in the radar beam) is composed of three classes: objects of interest, objects which are not of interest, and (known) background. Objects of interest are referred to as *targets*, while those objects which are not of interest are referred to as *clutter*. In our current exposition, we seek to minimize scattering from clutter by modifying the waveforms that are being transmitted into the scene. This is an important task, as scattering from clutter can overpower scattering from targets, rendering the targets difficult to detect or image. *Waveform preconditioning* has been introduced in a series of papers by the authors as a way to modify transmit waveforms for better performance in a cluttered environment [1]–[4]. Here, we will present the appropriate proofs for our previous results, thus providing a firm theoretical background for our waveform preconditioning work.

Waveform preconditioning involves determining a filter on the space of transmit waveforms. We refer to this filter as a *preconditioning operator*; it is applied to the transmit waveform prior to transmission. Our primary application is radar imaging. However, our physics-based approach, where we formulate the problem in terms of Green's functions and second-order random fields, is applicable to pulse-echo imaging in general, including ultrasound, sonar and microwave imaging.

It has long been recognized that the transmit waveforms impact the performance of radar systems. Early contributions to the field of waveform design was made by Wilcox [5], who considered waveforms which lead to good range- and Doppler resolution, and DeLong [6], Rummler [7], and Spafford [8], who tailored waveforms to the detection of point targets. There are currently two main waveform design approaches in the radar literature: ambiguity-based and variational-based. In the first approach, a range-Doppler echo model is used with matched-filter processing. The waveforms are designed and combined in order to create an approximate Dirac-delta ambiguity function [9]–[17]. In the second approach, the scene is assumed to be static, and therefore, range-only echo models are considered. Similar to the first approach, matched filtering is used as a foundation for joint design of waveforms and receive processing for target detection, identification and classification [18]–[21]. For target detection, the waveforms are designed by maximizing the signal-to-noise or signal-to-interference ratios [19]–[21]. A mutual information criteria has also been used to design optimal waveforms for target classification [19].

From a communications point of view, the radar transmit signal which illuminates the target may be considered as a means for establishing a *communication channel between the target and the observer*. In this language, the effect of a complex environment is considered as part of this communication channel. A filter is then designed, which, when applied to the transmit signal, shapes the received signal in a desired manner. There are therefore similarities between the ideas presented here for pulse-echo, and the existing literature on *precoding* [22]–[24]. However, since our primarily aim is to reconstruct the spatial distribution of the target, the spatial aspects of the wave propagation are pronounced in our work.

We derive clutter-rejecting waveforms for pulse-echo measurements from a sparse array of transmitting and receiving elements. The array elements can be distributed spatially in an arbitrary fashion, and can be several hundred wavelengths apart. Such an array is referred to as a *distributed aperture* [25]. Distributed apertures typically view regions of interest that are not in the far-field of the array. This introduces range-dependence in the scattering measurements which cannot be ignored [26], [27]. By using a physics-based measurement model we directly account not only for this range-dependence but also for effects such as multi-path scattering and interference. We incorporate *a priori* statistical information about the scatterers. Furthermore, we allow for multiple transmitters and receivers to be activated simultaneously [28]–[31], and make no additional assumptions about being able to separate the waveforms from each transmitter

by orthogonality [28], [32].

Our analysis leads to explicit expressions for the preconditioning operator involving the Green's function for the background medium, as well as second-order statistics for the target of interest and the clutter. It turns out, however, that the need for such explicit information can be relaxed by application of the time-reversal principle. The *time-reversal principle* is based on an invariance to changing the sign of the temporal variable in the wave equation [33], [34]. It has been used in many applications which involve wave propagation, *e.g.*, ultrasound imaging [34]–[37], underwater acoustics [38], [39], radar imaging [40], [41], and microwave imaging [42]. Typically, the time-reversal principle is applied successfully to cases where we have a multiple-scattering medium and where explicit modeling of the medium is difficult due to its complexity or due to random perturbations [37], [43]–[45]. Here, we show how the time-reversal principle can be employed to obtain the preconditioning operator when explicit models for the environment and/or the target and clutter distributions are not available.

Our paper is organized as follows: in Sec. II, we define *target* and *clutter*, as well as a *signal model* which relates *transmit waveforms* to *scattering measurements*. In the same section we also introduce a Hilbert-space structure which allows us to work with our stochastic scattering operators within the framework of Hilbert-Schmidt operators. In Sec. IV-B, we present the concept of waveform preconditioning, and the *waveform preconditioning operator*. We proceed to show that the waveform preconditioning operator may be evaluated using the time-reversal principle in Sec. V. In Sec. VI we present a numerical simulation indicating how waveform precondition would work. Section VII contains discussion and concluding remarks.

II. Preliminary Theory and Modeling

A. Notational Conventions

Throughout this paper we use the following font conventions: bold-face italic font ($\boldsymbol{x}$) denotes vector quantities, Latin capital letters in calligraphic font ($\mathcal{H}$) are used for operators, and Latin capital letters in roman font (S) are used to denote function spaces. We use subscript index (G_{ij}, x_i) to indicate a matrix or a vector element, while we reserve superscript indices (x^k) for indexing a set of vectors. We define the Fourier transform of a function f as

$$\hat{f}(\omega) := \frac{1}{2\pi}\int_{-\infty}^{\infty} f(x)\mathrm{e}^{-\mathrm{i}\omega t}dt \tag{1}$$

Our notation for specific variables, operators, functions and function spaces is shown in Table II-A.

B. Model for Distributed Aperture

We consider an antenna array consisting of m transmitting elements, and n receiving elements. The placement of these elements can be chosen arbitrarily; the location of each element may be assigned independently of where the other elements are located. For simplicity, we assume each element to behave like an isotropic point antenna; the radiation patterns

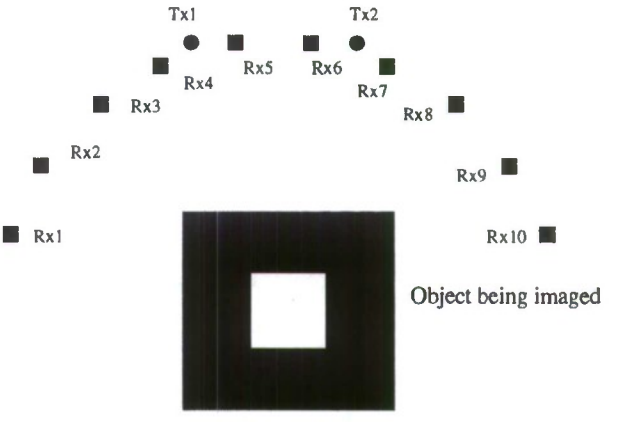

Fig. 1. Distributed array with two transmitting elements (circles labeled Tx_1 and Tx_2), and ten receiving elements (small squares labeled from Rx_1 to Rx_{10}). The elements are placed at equidistant points along an arc with radius 10λ, where λ is the wavelength corresponding to the center frequency of the transmitters. The target is indicated as a square with sides of 1.5λ, while the region of interest is $5\lambda \times 5\lambda$ around the target.

from each element do not exhibit any directivity. The latter assumption is not needed, but is made in order to keep the analysis more transparent. An important feature of the system under consideration is that we have a reference clock which is common to all of the elements. This common reference clock facilitates *coherent data processing*. An illustration of the distributed nature of an antenna with two transmitting elements and ten receiving elements is shown in Fig. 1.

In order to exploit the spatial diversity inherent in the antenna, it is desirable to allow for transmitting different waveforms from each element. Let $s_j(t)$ denote the waveform which emanates from the j^{th} element. The transmit waveforms are arranged in a *transmit vector* $\boldsymbol{s}(t)$

$$\boldsymbol{s}(t) := [s_1(t), \ldots, s_m(t)]^{\mathrm{T}}. \tag{2}$$

Similarly, if the measured scattering at the i^{th} receive element is denoted by $m_i(t)$, then the scattering which is collected by the distributed antenna may be arranged in a *measurement vector* $\boldsymbol{m}(t)$

$$\boldsymbol{m}(t) := [m_1(t), \ldots, m_n(t)]^{\mathrm{T}}. \tag{3}$$

C. Model for Multi-path Scattering

The ability to distinguish scattering objects depends on how much their electromagnetic properties deviate from a known background. We denote this deviation by the reflectivity function $V(\boldsymbol{x})$. At an abstract level, we denote by $\mathcal{H}(V)$ the operator which maps the transmit vector $\boldsymbol{s}(t)$ to the measurement vector $\boldsymbol{m}(t)$

$$\boldsymbol{m}(t) = \mathcal{H}(V)\boldsymbol{s}(t). \tag{4}$$

$\mathcal{H}(V)$ is called a scattering operator. An explicit relationship between V and $\mathcal{H}(V)$ can be derived in terms of the *Green's function* $g(\boldsymbol{x}, \boldsymbol{y}, t)$ for the background medium. The Green's function is the response measured at position $\boldsymbol{x}$ from an impulse $\delta(t)$ at position $\boldsymbol{y}$. The geometric layout of the antenna

Notation	Explanation
T_0	Positive constant which determines the maximum length of a transmit signal
V, T, C	Reflectivity functions
R_V, R_T, R_C	Covariance functions for reflectivity functions V, T and C, respectively
$\mathrm{S}(0,T_0)$	Space of transmit waveforms
$\mathrm{S} = \mathrm{S}(0,T_0)^m$	Space of transmit vectors
$\boldsymbol{s}(t)$	Transmit vector with vector elements in $\mathrm{S}(0,T_0)$
$\boldsymbol{m}(t)$	Measurement vector with vector elements in $L^2(\mathbb{R})$
$\mathcal{H}(V)$	Scattering operator: operator from $\mathrm{S}(0,T_0)^m$ to $L^2(\mathbb{R})^n$
$\mathcal{G}$	Green's function operator: operator which models scattering from an ideal point reflector
$\mathrm{Tr}\{\mathcal{A}\}$	Trace of the operator $\mathcal{A}$
Ω	Compact subset of $\mathbb{R}^3$ where all reflectivity functions have support

TABLE I
DEFINITION OF VARIABLES, OPERATORS, FUNCTIONS, AND FUNCTION SPACES.

elements naturally plays an important role here. Let therefore the j^{th} transmit element be located at position $\boldsymbol{z}_j$, and the i^{th} receive element be located at position $\boldsymbol{x}_i$. In the current analysis we use a linear scattering model often known as the *distorted-wave Born approximation* [46]. If we define a $(m \times n)$ matrix $G(\boldsymbol{y}, t)$ with matrix elements

$$G_{ij}(\boldsymbol{y}, t) := \int g(\boldsymbol{x}_i, \boldsymbol{y}, \tau')\partial_t^2 g(\boldsymbol{y}, \boldsymbol{z}_j, t-\tau')\mathrm{d}\tau', \quad (5)$$

then

$$\mathcal{H}(V)\boldsymbol{s}(t) := \int G(\boldsymbol{y}, t-\tau)V(\boldsymbol{y})\mathrm{d}\boldsymbol{y}\ \boldsymbol{s}(\tau)\mathrm{d}\tau. \quad (6)$$

Integration in Eq.(6) is understood to be element-wise. For a derivation of Eq. 6, we refer to the Appendix of [47].

We use the notation $\mathcal{G}$ for the integral operator with (matrix) kernel $G(\boldsymbol{y}, t, \tau)$ where the elements of G are given in Eq.5

$$\mathcal{G}\boldsymbol{f}(\boldsymbol{y}, t) := \int G(\boldsymbol{y}, t-\tau)\boldsymbol{f}(\tau)\mathrm{d}\tau. \quad (7)$$

In many situations it is reasonable to assume that information about statistics of the scattering is available. There is a large body of literature on stochastic signal models for electromagnetic waves (see *e.g.*, Sarkar *et al.* [48] and the references therein). Here, we have chosen to impose a stochastic model for the reflectivity function. More specifically, we make the following assumptions:

Assumption 1. *The reflectivity function $V(\boldsymbol{y})$ is a zero-mean random field with continuous covariance function*

$$R_V(\boldsymbol{x}_1, \boldsymbol{x}_2) = \mathbb{E}\left[V(\boldsymbol{x}_1)\overline{V(\boldsymbol{x}_2)}\right]. \quad (8)$$

Let Ω be a fixed compact subset of $\mathbb{R}^3$, and let K be a fixed constant.

1) *All scattering takes place at locations inside Ω. More precisely, we assume that $R_V(\boldsymbol{x}, \boldsymbol{x})$ is supported in Ω. In addition, we assume for simplicity that each realization of V is in $L^2(\Omega)$.*
2) *All transmitter locations $\boldsymbol{z}^j$ and receiver locations $\boldsymbol{x}^i$ are outside Ω.*
3) *The background medium does not focus energy onto an arbitrarily small region; in other words, we rule out trapped rays. More precisely, let $\hat{g}(\boldsymbol{x}, \boldsymbol{y}, \omega)$ denote the temporal Fourier transform of the Green's function $g(\boldsymbol{x}, \boldsymbol{y}, t)$. We assume that*

$$\left|\hat{g}(\boldsymbol{x}^i, \boldsymbol{y}, \omega)\hat{g}(\boldsymbol{y}, \boldsymbol{z}^j, \omega)\right| \leq K, \quad (9)$$

uniformly for all frequencies $\omega \in \mathbb{R}$, all $\boldsymbol{y} \in \Omega$, and all pairs of transmitter and receiver locations $(\boldsymbol{z}^j, \boldsymbol{x}^i)$.

Parts *(2)* and *(3)* of Assumption 1 can be relaxed somewhat. However, this would require additional attention to deal with the integrable singularities of the Green's function. We also note that the background may always be defined in such a way that the first-order statistics of the reflectivity function is zero. Therefore, the zero-mean assumption can be made without loss of generality.

The fact that the reflectivity function is a random field, of course, implies that the kernel of the integral operator in Eq.(6) is stochastic [49, Ch.2].

D. Model for Target and Clutter

The above formalism allows us to utilize a physics-based model for the background, which in principle can contain an arbitrary level of detail. It is not reasonable, however, to expect that the background model can account for all details of the scene except for the target. As outlined in the introduction, this suggests that the reflectivity function should be divided into two parts

$$V(\boldsymbol{x}) = T(\boldsymbol{x}) + C(\boldsymbol{x}), \quad (10)$$

where $T(\boldsymbol{x})$ represents *target* and $C(\boldsymbol{x})$ represents *clutter*. Note that our definition of clutter incorporates contributions due to a compromise between model fidelity and tractability: clutter includes deviations between the background and our model for the background. The real interest lies in recovering T, while suppressing C.

For our purpose it is reasonable to assume that target and clutter are independent of each other:

Assumption 2. *Let V satisfy Assumption 1, and let T and C be related to V through Eqn.10. We assume that T and C are:*

1) *zero-mean random fields with continuous covariance*

functions

$$R_T(\boldsymbol{x}_1, \boldsymbol{x}_2) = \mathbf{E}\left[T(\boldsymbol{x}_1)\overline{T(\boldsymbol{x}_2)}\right] \tag{11}$$

$$R_C(\boldsymbol{x}_1, \boldsymbol{x}_2) = \mathbf{E}\left[C(\boldsymbol{x}_1)\overline{C(\boldsymbol{x}_2)}\right]. \tag{12}$$

2) *statistically independent such that*

$$R_V(\boldsymbol{x}_1, \boldsymbol{x}_2) = R_T(\boldsymbol{x}_1, \boldsymbol{x}_2) + R_C(\boldsymbol{x}_1, \boldsymbol{x}_2). \tag{13}$$

We briefly note that since $R_V(\boldsymbol{x}, \boldsymbol{x})$ is supported on Ω, so are $R_T(\boldsymbol{x}, \boldsymbol{x})$ and $R_C(\boldsymbol{x}, \boldsymbol{x})$. Furthermore, it follows that R_V, R_T and R_C are all supported on $\Omega \times \Omega$.

We use the notation $\mathcal{R}_T$ and $\mathcal{R}_C$ for integral operators with (scalar) kernels R_T and R_C from Eqns. 11 and 12, respectively

$$\mathcal{R}_T f(\boldsymbol{y}_1) := \int R_T(\boldsymbol{y}_1, \boldsymbol{y}_2) f(\boldsymbol{y}_2) \mathrm{d}\boldsymbol{y}_2 \tag{14}$$

$$\mathcal{R}_C f(\boldsymbol{y}_1) := \int R_C(\boldsymbol{y}_1, \boldsymbol{y}_2) f(\boldsymbol{y}_2) \mathrm{d}\boldsymbol{y}_2. \tag{15}$$

III. Strategy for Clutter Rejection and Image Formation

In this section we briefly outline our strategy for clutter rejection and image formation.

A. Clutter Rejection

Our goal is to suppress C by modifying the transmit waveforms such that they produce mostly scattering from T. Loosely speaking, this is achieved by determining a deterministic (linear) operator $\mathcal{W}$ on the space of transmit waveforms such that

$$\mathcal{H}(T + C)\mathcal{W} \approx \mathcal{H}(T). \tag{16}$$

We suppress scattering from C by employing the transmit waveform $\mathcal{W}\boldsymbol{s}(t)$ instead of $\boldsymbol{s}(t)$. We refer to the operator $\mathcal{W}$ as the *preconditioning operator*. The design of the preconditioning operator is discussed in sections IV and V.

B. Image Formation

We obtain an image by inverting the mapping $\mathcal{H} : T \mapsto \mathcal{H}(T)$, *i.e.*, we reconstruct the target reflectivity function T from the knowledge of $\mathcal{H}(T)$. The inversion is performed by the following steps.

1) We approximate the inverse of $\mathcal{H}$ via the pseudo-inverse $\mathcal{H}^\dagger = (\mathcal{H}^*\mathcal{H})^{-1}\mathcal{H}^*$, where $\mathcal{H}^*$ denotes the adjoint. Note that $\mathcal{H}$ depends only on the known background medium, so $\mathcal{H}^\dagger$ can be computed off-line.
2) We do a singular value decomposition (SVD) of $\mathcal{H}^*\mathcal{H}$, denoting the singular values by λ_n and the singular vectors by U_n. Since $\mathcal{H}$ and $\mathcal{H}^*\mathcal{H}$ operate on "vectors" consisting of scenes, the singular "vectors" U_n consist of elemental scattering scenes. Again, because $\mathcal{H}$ is known, this step can be done off-line.
3) We construct the scattering operators $\mathcal{U}_n = \mathcal{H}(U_n)$ corresponding to the elemental scenes. In other words, we compute the scattering data corresponding to the elemental scenes. This too can be done off-line.
4) We take the inner product of each measurement vector $\boldsymbol{m}$ with the predicted measurements due to scattering from each elemental scene $\mathcal{U}_n \boldsymbol{s}$.
5) From the SVD of $\mathcal{H}^*\mathcal{H}$, we have the general formula for any scene Y:

$$(\mathcal{H}^*\mathcal{H})^\dagger Y = \sum_n \frac{1}{\lambda_n}\langle Y, U_n\rangle U_n \tag{17}$$

Consequently, we can compute the image $\tilde{T}$ as

$$\tilde{T} = \underbrace{(\mathcal{H}^*\mathcal{H})^\dagger \mathcal{H}^*}_{\text{pseudoinverse}} \underbrace{[\mathcal{H}(T)]}_{\text{data}} = \sum_n \frac{1}{\lambda_n}\langle [\mathcal{H}^*\mathcal{H}(T)], U_n\rangle U_n \tag{18}$$

where we have used (17) with $Y = \mathcal{H}^*\mathcal{H}(T)$. In (18), the inner product is computed as

$$\begin{aligned}\langle [\mathcal{H}^*\mathcal{H}(T)], U_n\rangle &= (\mathcal{H}(T), \mathcal{H}(U_n)) \\ &= \sum_{k=1}^{K} (\mathcal{H}(T)\boldsymbol{s}^k, \mathcal{H}(U_n)\boldsymbol{s}^k) \\ &= \sum_{k=1}^{K} (\boldsymbol{m}^k, \mathcal{H}(U_n)\boldsymbol{s}^k)\end{aligned} \tag{19}$$

Here we have used the definition given in section A of the inner product of two Hilbert-Schmidt operators.

In summary, once we have precomputed U_n, $\mathcal{H}(U_n)\boldsymbol{s}^k$, and λ_n, we simply take inner products of the measured data $\boldsymbol{m}^k = \mathcal{H}(T)\boldsymbol{s}^k$ with $\mathcal{H}(U_n)\boldsymbol{s}^k$ as in (19) and form the sum (18).

More detail, including extension of this basic idea to stochastic T, can be found in [47].

IV. Preconditioning Operator

In this section we identify a Hilbert-space structure for scattering. We next use this Hilbert space structure to design a preconditioning operator for clutter rejection.

A. Hilbert-space Structure

In this section we identify a Hilbert-space structure for the transmitted waveforms and the scattering operator.

1) The Hilbert space $\mathrm{S}(0, T_0)$ of transmit waveforms: We assume that the transmit waveforms have finite energy, are of finite duration, and are approximately band-limited in the sense that their Fourier transforms decay rapidly. More specifically, let $\rho > 0$ and $T_0 > 0$ be predetermined constants. The space $\mathrm{S}(0, T_0)$ of transmit waveforms is a subset of the Sobolev space $\mathring{\mathrm{H}}^{(5+\rho)/2}(0, T_0)$. Here $\mathrm{H}^{(5+\rho)/2}(\mathbb{R})$ consists of functions s whose Fourier transforms $\hat{s}(\omega)$ satisfy

$$\int (1 + |\omega|^{5+\rho})|\hat{s}(\omega)|^2 \mathrm{d}\omega < \infty \tag{20}$$

and $\mathring{\mathrm{H}}^{(5+\rho)/2}(0, T_0)$ is the subspace of $\mathrm{H}^{(5+\rho)/2}(\mathbb{R})$ of functions with support in $[0, T_0]$. On the space $\mathrm{S}(0, T_0)$, we use the $\mathrm{H}^{(5+\rho)/2}(\mathbb{R})$ inner product

$$\langle f, g\rangle_{\mathrm{S}} := \int (1 + |\omega|^{5+\rho})\hat{f}(\omega)\overline{\hat{g}(\omega)}\mathrm{d}\omega. \tag{21}$$

For the transmit waveform vector, we consider the direct product $S = \mathrm{S}(0, T_0)^m$ of $\mathrm{S}(0, T_0)$.

2) The Hilbert space of scattering operators: For each realization of the reflectivity function V in $\mathrm{L}^2(\Omega)$, the scattering operator $\mathcal{H}(V)$ is a Hilbert-Schmidt [50, Ch. 6.2] map between the Hilbert space S and $[L^2(\mathbb{R})]^n$ (Lemma 1 in Varslot *et al.* [47]). For the definition of an HS operator, see Appendix A.

B. The Design of the Preconditioning Operator

We determine a linear preconditioning operator $W : \mathrm{S} \to \mathrm{S}$ by minimizing the expected Mean Square Error (MSE):

$$\mathcal{W} := \underset{\mathcal{W}}{\operatorname{argmin}}\ \mathbb{E}\|\mathcal{H}(T+C)\mathcal{W} - \mathcal{H}(T)\|_{\mathrm{HS}}^2. \tag{22}$$

Here the HS norm is computed for each realization, and the resulting values are averaged over all realizations.

Theorem 1. *The linear operator $\mathcal{W}$ which solves Eq. 22, and hence minimizes the MSE of the approximation in Eq. 16 is*

$$\mathcal{W} = [\mathbb{E}[\mathcal{H}(T+C)^*\mathcal{H}(T+C)]]^\dagger\, \mathbb{E}\,[\mathcal{H}(T)^*\mathcal{H}(T)]\,. \tag{23}$$

Here $*$ denotes adjoint involving the inner products $\langle\cdot,\cdot\rangle_2$ in $[L^2]^n$ and $(\cdot,\cdot)_{\mathrm{S}}$, and $\dagger$ denotes (Moore-Penrose) pseudo-inverse. The operator $\mathcal{W}$ can be alternatively expressed as

$$\mathcal{W} = [\mathcal{G}^*[\mathcal{R}_T + \mathcal{R}_C]\mathcal{G}]^\dagger\ [\mathcal{G}^*\mathcal{R}_T\mathcal{G}]\,. \tag{24}$$

where $\mathcal{G}^*$ is the adjoint of $\mathcal{G}$ with respect to standard inner products in $(\mathrm{L}^2)^m$ and $(\mathrm{L}^2)^n$.

We prove this theorem in the Appendix B.

The operator $\mathcal{W}$ may be applied to any transmit vector in S to yield a new transmit vector; $\mathcal{W}$ is a bounded linear operator in this space. Loosely speaking, $\mathcal{W}$ emphasizes subspaces of S which result in best signal-to-clutter ratio.

V. Time-Reversal Preconditioning

Although Theorem 1 gives an explicit expression for the preconditioning operator, computing the operator is difficult, as it requires a priori information about the second-order statistics of target and clutter, as well as a model for the background medium. In this section, we introduce a time-reversal experiment which allows us to estimate the preconditioning operator from scattering measurements directly eliminating the need for a priori information.

First, from Eq. (6) we see that $\mathcal{H}(T+C) = \mathcal{H}(T) + \mathcal{H}(C)$. We use this fact to write

$$\mathcal{H}(T) = \mathcal{H}(T+C) - \mathcal{H}(C). \tag{25}$$

Inserting Eq. (25) into Eq.(23) we arrive at

$$\mathcal{W} = I - [\mathbb{E}[\mathcal{H}(T+C)^*\mathcal{H}(T+C)]]^\dagger\ \mathbb{E}\,[\mathcal{H}(C)^*\mathcal{H}(C)] \tag{26}$$

$$= I - [\mathcal{G}^*(\mathcal{R}_T + \mathcal{R}_C)\mathcal{G}]^\dagger\mathcal{G}^*\mathcal{R}_C\mathcal{G}. \tag{27}$$

The last equality follows from Eq. 24 The significant difference between Eq. (23) and (26) is that in Eq. (26) we have replaced $\mathcal{H}(T)^*\mathcal{H}(T)$ by $\mathcal{H}(C)^*\mathcal{H}(C)$. This is important, as $\mathcal{H}(T)$ corresponds to scattering from a target without the presence of clutter, and is infeasible to measure. On the other hand, $\mathcal{H}(C)$ corresponds to scattering from clutter. This can be observed at times when there is no target present.

Consider now the case where there is no target present, and let $c_k(x)$ be a particular clutter realization. By definition, the measured scattering we obtain is $\boldsymbol{m}^k(t) = \mathcal{H}(c_k)\boldsymbol{s}(t)$. Furthermore, if we interchange the roles of transmitters and receivers, and transmit $\boldsymbol{m}^k(-t)$, this corresponds to employing the transpose of the matrix kernel G in Eq. (6), *i.e.*, the measured responses at the original transmitters become

$$q_k(t) = \int G^{\mathrm{T}}(\boldsymbol{y}, t-\tau)c_k(y)\mathrm{d}\boldsymbol{y}\ \boldsymbol{m}^k(-\tau)\mathrm{d}\tau. \tag{28}$$

If we now insert Eqns. 6 into Eq. 28, and express it in the temporal frequency domain, we obtain

$$\hat{q}^k(\omega) = \int \hat{G}^{\mathrm{T}}(\boldsymbol{y},\omega)c_k(\boldsymbol{y})\mathrm{d}\boldsymbol{y}\ \overline{\hat{\boldsymbol{m}}(\omega)} \tag{29}$$

$$= \int \hat{G}^{\mathrm{T}}(\boldsymbol{y},\omega)c_k(\boldsymbol{y})\mathrm{d}\boldsymbol{y}\ \overline{\int \hat{G}(x,\omega)c_k(x)\mathrm{d}x\hat{\boldsymbol{s}}(\omega)} \tag{30}$$

$$= \overline{\int \hat{G}^{\mathrm{H}}(\boldsymbol{y},\omega)\overline{c_k(\boldsymbol{y})}c_k(x)\hat{G}(x,\omega)\mathrm{d}x\mathrm{d}\boldsymbol{y}\hat{\boldsymbol{s}}(\omega)}. \tag{31}$$

Consider now averaging this experiment over multiple realizations of the clutter to form

$$p(t) := \frac{1}{N}\sum_{k=1}^{N} q^k(-t). \tag{32}$$

Then

$$p(t) = \frac{1}{N}\sum_{k=1}^{N}\int \hat{G}^{\mathrm{H}}(\boldsymbol{y},\omega)\overline{c_k(\boldsymbol{y})}c_k(x)\hat{G}(x,\omega)\mathrm{d}x\mathrm{d}\boldsymbol{y}\hat{\boldsymbol{s}}(\omega) \tag{33}$$

$$\approx \int \hat{G}^{\mathrm{H}}(\boldsymbol{y},\omega)\mathbb{E}\left[\overline{c_k(\boldsymbol{y})}c_k(x)\right]\hat{G}(x,\omega)\mathrm{d}x\mathrm{d}\boldsymbol{y}\hat{\boldsymbol{s}}(\omega) \tag{34}$$

$$= \int \hat{G}^{\mathrm{H}}(\boldsymbol{y},\omega)R_C(x,\boldsymbol{y})\hat{G}(x,\omega)\mathrm{d}x\mathrm{d}\boldsymbol{y}\hat{\boldsymbol{s}}(\omega). \tag{35}$$

Comparing this expression with the frequency-domain expression for $\mathcal{G}^*\mathcal{R}_C\mathcal{G}\boldsymbol{s}(t)$, we see that $p(t)$ is an approximation for $\mathcal{G}^*\mathcal{R}_C\mathcal{G}\boldsymbol{s}(t)$.

Under the assumption that there is no target present in the scene, the following algorithm allows us to obtain $\mathcal{G}^*\mathcal{R}_C\mathcal{G}$ applied to a transmit vector $\boldsymbol{s}$:

1) Transmit waveform $\boldsymbol{s}(t)$ and obtain measurement $\boldsymbol{m}^k(t)$.
2) Interchange the role of transmitters and receivers
3) Transmit waveform $\boldsymbol{m}^k(-t)$ and obtain measurement $q^k(t)$.
4) Repeat multiple times to obtain the estimate

$$p(t) = \frac{1}{N}\sum_{k=1}^{N} q_k(-t) \approx \mathcal{G}^*\mathcal{R}_C\mathcal{G}\boldsymbol{s}(t)\boldsymbol{s}(t).$$

The same procedure allows us to determine $\mathcal{G}^*(\mathcal{R}_T + \mathcal{R}_C)\mathcal{G}\boldsymbol{s}(t)$ from data containing scattering from both target and clutter. We can thus estimate the required information for computing $\mathcal{W}$ as defined in Eq. 27.

Finally, to carry out the imaging process, we transmit $\mathcal{W}\boldsymbol{s}$, obtain the corresponding measurements, and use these

measurements to construct an approximation to $\mathcal{H}(T)$. This is used in the imaging algorithm outlined in section III.

VI. Numerical Simulation

In order to demonstrate the clutter-suppression obtained with our waveform preconditioning operator, we have performed a set of numerical simulations. In these simulations we want to image the target T from scattering measurements made with two transmitters and ten receivers. The transmitters and receivers were placed equally spaced on an arc around the target. This simulation setup is illustrated in Fig. 1.

We employed the imaging method proposed in [47] to form the images. This method is well suited to work with waveform preconditioning, as it is capable of handing scattering from multiple sources simultaneously, and is based on the same figure of merit as our current preconditioning work; it forms the optimal image in a MSE sense.

From the two transmitters we transmitted short chirp signals: transmitter 1 emitted a linear up-chirp, while transmitter 2 simultaneously emanated a linear down-chirp. The dimensions of the experiment was normalized according to the wavelength corresponding to the center frequency. We denote this wavelength by λ.

As a target we chose a square with sides $1.5\lambda \times 1.5\lambda$. From this target model we constructed a target spectrum as if the target was a realization of a stationary random field. A high-frequency version of the stationary stochastic target model was then constructed and used to simulate different realizations of the surrounding clutter. This construction is explained further in Yazıcı *et al.* [51]. Compact support of the clutter was imposed by subsequently applying a spatial mask, rendering the clutter inherently non-stationary. For our purpose we used a region of $5\lambda \times 5\lambda$ around the target as our compact set Ω. The radius of the arc on which the antenna elements were placed was set to 10λ.

The preconditioning operator was constructed according to Eq.(23) by a Monte-Carlo approach where we used 500 realizations of T and C. The spatial discretization for each scattering simulation was 15 samples per wavelength λ.

The signal-to-clutter ratio (SCR) in our simulations was set to -3.5 dB, when defined according to

$$\mathrm{SCR} = 10\log\left(\frac{\int \mathbb{E}\left[|T(x)|^2\right]\mathrm{d}x}{\int \mathbb{E}\left[|C(x)|^2\right]\mathrm{d}x}\right). \tag{36}$$

The performance of the preconditioning was then evaluated by observing the square error in the reconstructed image when compared to the true scattering potential. The mean-square-error (MSE) was estimated by averaging over 10 clutter realizations. We computed the MSE according to

$$\mathrm{MSE}(\mathcal{W}) = \tag{37}$$
$$10\log\left(\frac{\int \mathbb{E}\left[|[\mathcal{H}^{-1}\mathcal{H}(T+C)\mathcal{W}](x) - T(x)|^2\right]\mathrm{d}x}{\int \mathbb{E}\left[|T(x)|^2\right]\mathrm{d}x}\right).$$

Here $\mathcal{H}^{-1}$ simply indicates our imaging algorithm. The images were reconstructed on a grid with 10 samples per wavelength. We used a reconstruction algorithm which is consistent with clutter rejection in the MSE sense; for a given scattering measurement, the algorithm minimizes the MSE in the reconstruction [47].

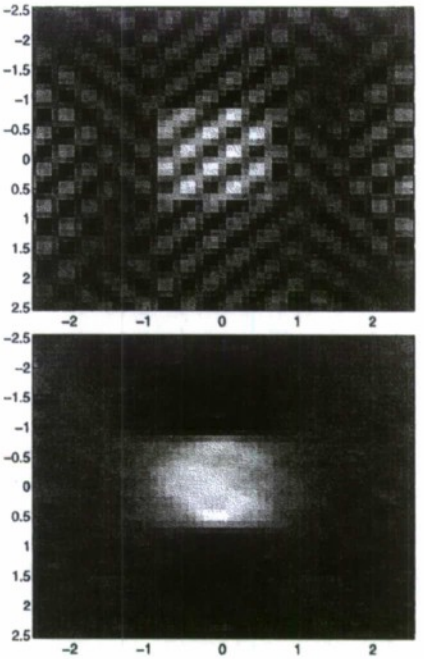

Fig. 2. Target with clutter (left) and reconstruction of target from clutter-free scattering (right).

Figure 2 shows the target embedded in clutter, as well as a reconstructed image based on scattering without clutter in free space. The MSE is in this case was -3.7 dB. The latter is used to give an indication of the best-case performance of the imaging algorithm for this scenario.

Figure 3 shows reconstruction result for a particular realization of the clutter. Preconditioning of the transmit waveform improves image quality from 1.1 dB to -3.6 dB when measured using the MSE defined in Eq.(37).

Figure 4 shows the spectrum of one of the transmit waveform that were employed in this experiment.

VII. Conclusions

In this work we separated the reflectivity function into two distinct classes: ***target*** and ***clutter***. The clutter produces unwanted scattering which in turn degrades the final result of the reconstructed image. If scattering from clutter can be removed from the measurement, the end result will be improved.Our preconditioning operator can be applied to any set of transmit vectors in order to optimally reject scattering from clutter in an MSE sense.

When we perform clutter rejection, we implicitly identify a transmit-vector subspace where the signal-to-clutter (SCR) ratio is high. The fact that we allow for waveforms to be transmitted simultaneously, and that they are not orthogonal imply that there is a great deal of ambiguity in the data with respect to the correct time-of-flight for a given echo. We

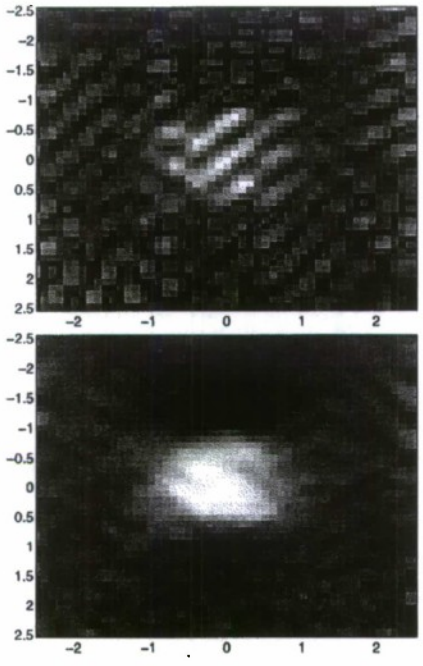

Fig. 3. Reconstruction results for a single realization of clutter. Left: image from scattering with original chirp waveform. Right: image from scattering with preconditioned chirp waveform.

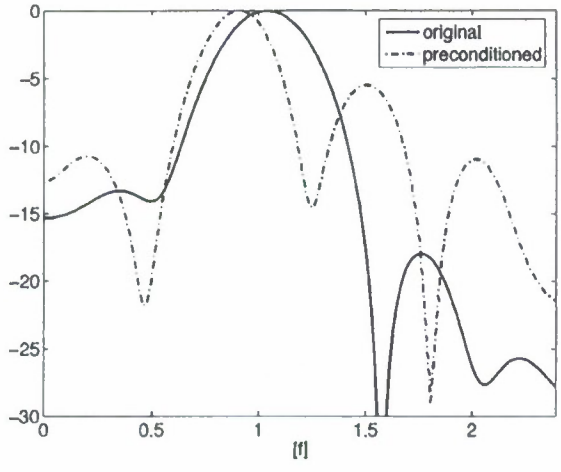

Fig. 4. Spectrum of transmit waveforms.

therefore have limited ability to determine the correct source-receiver pair for a given echo. Our choice of imaging algorithm reflects this, in that it does not rely on the ability to resolve the source-receiver ambiguity [47].

Our analysis is based on assumed *a priori* knowledge about the scene in the form of the Green's function, and about the target and clutter distribution in the form of first and second-order statistics. We used the Green's function to map second-order statistics of the clutter and target to the space of transmit vectors and thereby construct the preconditioning operator. Finally, we point out how the time-reversal principle can be applied to alleviate the need for explicit knowledge about the Green's function and the target/clutter statistics.

We address the problem of modifying the transmit waveform when the transmit power is limited. Obviously, after preconditioning the resulting waveform may not have the same strength. However, this is trivially amended by proper normalization of the preconditioned waveform. As a result, the transmit vector contains the same power as the original transmit waveform, but its shape is modified to minimize scattering from clutter. Hence, for a fixed total transmit power, the SCR may be improved in the final image. Alternatively, for a given signal-to-noise ratio in the final image the total transmit power can be reduced. This is of interest in applications where it is desirable to keep the transmit power as low as possible, *e.g.*, to reduce transmitter vulnerability/detectability.

The underlying propagation model which we have used for this work is derived from a scalar wave equation. This is a commonly-used model for many radar applications where polarization effects may be ignored. In order to get explicit expressions in terms of Green's functions, a linearized scattering model was used, namely the distorted-wave Born approximation (DWB). Note, however, that the operator norm which we used to determined the preconditioning operator also makes sense without the DWB. Furthermore, the time-reversal principle also holds in other pulse-echo applications. Our work therefore has applications also in other areas such as ultrasound, sonar and microwave imaging.

Clutter filtering process is an integral part of *space-time adaptive processing* (STAP). In STAP the statistics of the clutter is used to perform filtering of the measurement in order to reduce the clutter content. [52] Filtering of the measurements implies that parts of the scattered power do not contribute to the final result. In this sense, filtering clutter in receive results in waste of scattering power. We obtain a similar result by filtering the transmit signal, thereby avoiding transmitting power which is predominantly used to produce scattering from clutter. In this sense, the preconditioned transmit vector yields more efficient use of the transmitter power. By avoiding clutter filtering of the measurements, we reduce the computational resources needed at each the receiver element. Our scheme is therefore suited for applications where inexpensive receiver elements with limited computing power are employed, such as distributed sensing in urban environments.

The development in this paper was performed using the minimum-mean-square-error (MMSE) to define the optimal clutter rejection operator. This is a suitable in many applications. However, it should be possible to apply the idea of preconditioning in conjunction with other figures of merit, leading to different optimal preconditioning operator.

ACKNOWLEDGEMENTS

We are grateful to Air Force Office of Scientific Research[1] (AFOSR) and the Defense Advanced Research Projects

[1]Consequently, the US Government is authorized to reproduce and distribute reprints for governmental purposes notwithstanding any copyright notation thereon. The views and conclusions contained herein are those of the authors and should not be interpreted as necessarily representing the official policies or endorsements, either expressed or implied, of the Air Force Research Laboratory or the US Government.

Agency (DARPA) for supporting this work under the agreements FA9550-04-1-0223, FA9550-07-1-0363, FA9550-06-1-0017 and FA8750-05-2-0285.

REFERENCES

[1] B. Yazıcı and G. Xie, "Wideband extended range-Doppler imaging and waveform design in the presence of clutter and noise," *IEEE Trans. Inf. Theory* **52**(10), 2006.

[2] T. Varslot, B. Yazıcı, C. E. Yarman, M. Cheney, and L. Sharf, "Waveform preconditioning for clutter rejection," in *Proc. 2007 SPIE Defense and Security Conference*, p. 6568N, 2007.

[3] T. Varslot, B. Yazıcı, C. E. Yarman, M. Cheney, and L. Sharf, "Time-reversal waveform preconditioning for clutter rejection," in *Proc. 3rd International IEEE Conference in Waveform Design and Diversity*, p. 4016, 2007.

[4] T. Varslot, B. Yazıcı, C. E. Yarman, M. Cheney, and L. Sharf, "Waveform preconditioning for clutter rejection in multipath for sparse distributed apertures," in *Proc. of The Second International Workshop on Computational Advances in Multi-Sensor Adaptive Processing (COMSAP)*, December 2007.

[5] C. Wilcox, *The synthesis problem for radar ambiguity functions*, pp. 229–260. Springer-Verlag, 1991.

[6] D. F. DeLong and E. Hodstetter, "On the design of optimum radar waveforms for clutter rejection," *IEEE Trans. Inf. Theary* **13**(3), pp. 454–463, 1967.

[7] W. D. Rummler, "A technique for improving the clutter performance of coherent pulse train signals," *IEEE Tran. an Aeraspoce Electranic Systems* **AES-3**, pp. 898–906, 1967.

[8] L. Spafford, "Optimum radar signal processing in clutter," *IEEE Trans. Inf. Theory* **14**(5), pp. 734–743, 1968.

[9] R. H. Barker, *Group synchronizing of binary digital systems*, pp. 273–287. Academic Press, New York, 1953.

[10] R. L. Frank, "Polyphase codes with good nonperiodic correlation properties," *IEEE Trans. Inf. Theory* **9**(1), pp. 43–45, 1963.

[11] R. Sivaswamy, "Digital and analog subcomplementary sequences for pulse compression," *IEEE Trans. Aerosp. Electron. Syst.* **AES-14**, pp. 343–350, 1978.

[12] R. Sivaswamy, "Multiphase complementary codes," *IEEE Trans. Inf. Theory* **IT-24**(5), pp. 546–552, 1978.

[13] J. P. Costas, "A study of a class of detection waveforms having nearly ideal range-doppler ambiguity properties," *Proc. IEEE* **72**(8), pp. 996–1009, 1984.

[14] S. W. Golomb and H. Taylor, "Constructions and properties of costas arrays," *Proc. IEEE* **72**(9), pp. 1143–1163, 1984.

[15] S. W. Golomb and H. Taylor, "Algebraic construction of costas arrays," *J. Comb. Theory, ser. A* **37**, pp. 13–21, 1984.

[16] J. Guey and M. Bell, "Diversity waveform sets for delay-doppler imaging," *IEEE Transactions on Infarmation Theary* **44**(4), pp. 1504 – 1522, 1998.

[17] C. Chang and M. R. Bell, "Frequency-coded waveforms for enhanced delay-doppler resolution," *IEEE Trans. Inf. Theory* **49**(11), pp. 2960–2971, 2003.

[18] D. T. Gjessing, *Target Adaptive Matched Illumination Radar: Principles and Applications*, Peter Peregrinus, Stevenage, U.K., 1986.

[19] M. Bell, "Information theory and radar waveform design," *IEEE Trans. Inf. Theory* **39**, pp. 1578–1597, September 1993.

[20] S. U. Pillai, H. S. Oh, D. C. Youla, and J. R. Guerci, "Optimum transmit-receiver design in the presence of signal-dependent noise and channel noise," *IEEE Trans. Inf. Theary* **46**(2), pp. 577–584, 2000.

[21] D. A. Garren, M. K. Osborn, A. C. Odom, J. S. Goldstein, S. U. Pillai, and J. R. Guerci, "Enhanced target detection and identification via optimized radar transmission pulse shape," *Proc. IEE, Radar, Sanar and Navigation* **148**(3), pp. 130–138, 2001.

[22] G. Forney and M. Eyuboglu, "Combined equalization and coding using precoding," *IEEE Comm Mog* , Dec 1991.

[23] H. Harashima and H. Miyakawa, "Matched transmission technique for channels with intersymbol interference," *IEEE Trans. Commun.* **COM-20**, pp. 774–780, 1972.

[24] M. Tomlinson, "New automatic equalizer employing modulo arithmetic," *Electron. Lett.* **7**, pp. 138–139, 1971.

[25] R. Adve, R. Schneibler, G. Genello, and P. Antonik, "Waveform-space-time adaptive processing for distributed aperture radars," in *Proc. 2005 IEEE Radar Conf.*, pp. 93–97, 2005.

[26] R. Adve, R. Schneibler, and R. McMillan, "Adaptive space/frequency processing for distributed apertures," in *Proc. 2003 IEEE Radar Conf.*, pp. 160–164, 2003.

[27] R. Adve, "Sub-optimal adaptive processing for distributed aperture radars," in *Proc. 2nd Waveform Diversity Workshop*, pp. 160–164, (Verona, NY), 2003.

[28] E. Fishler, A. Haimovich, R. Blum, L. Cimini, D. Chizhik, and R. Valenzuela, "Spatial diversity in radars - models and detection performanee," *IEEE Trans. Sign. Processing* **54**(3), pp. 823–238, 2006.

[29] I. Bekkerman and J. Tabrikian, "Target detection and localization using MIMO radars and sonars," *IEEE Tran. Signal Proc.* **54**(10), pp. 3873–3883, 2006.

[30] A. Fletcher and F. Robey, "Performanee bounds for adaprive eoherenee of sparse array radar," in *Proc. of 11th. Conf. Adaptive Sensors Array Processing, Lexington (MA)*, March 2003.

[31] D. Rabideau, "Ubiquitous mimo digital array radar," in *Proc. 37th Asilomar Conf. Signals, Systems, Computers*, 2003.

[32] E. Bond, S. Hagness, and B. Veen, "Microwave imaging via space-time beamforming for early detection of breast cancer," *IEEE Trans. Ant. Prop.* **51**(8), pp. 1690–1705, 2003.

[33] M. Fink, "Time-reversed acoustics," *Scientific American* **281**, pp. 91–97, Nov 1999.

[34] M. Fink, "Time reversal of ultrasonic fields - part I: Basic prinsiples," *IEEE Trans. Ultrason. Ferroelectr. Freq. Cantrol* **39**, pp. 555–567, 1992.

[35] C. Prada, J. L. Thomas, and M. Fink, "The iterative time reversal process: analysis of eonvergenee," *J. Acoust. Soc. Am.* **97**, pp. 62–71, January 1995.

[36] M. Tanter, J.-L. Thomas, and M. Fink, "Time reversal and the inverse filter," *J. Acoust. Soc. Am.* **108**, pp. 223–234, July 2000.

[37] G. Montaldo, D. Palacio, M. Tanter, and M. Fink, "Building three-dimensional images using a time-reversal chaotic cavity," *IEEE Trans. Ultrasan. Ferroelectr. Freq. Control* **52**, pp. 1489–1497, September 2005.

[38] G. F. Edmann, H. C. Song, S. Kim, W. S. Hodgkiss, W. A. Kuperman, and T. Akal, "Underwater acoustic communications using time reversal," *IEEE J Oceanic Engineering* **30**(4), pp. 852–864, 2005.

[39] H. C. Song, W. S. Hodgkiss, W. A. Kuperman, M. Stevenson, and T. Akal, "Improvement of time-reversal communications using adaptive channel equalizers," *IEEE J Oceanic Eng.* **31**(2), pp. 487–496, 2006.

[40] D. Liu, G. Li, Y. Chen, S. Vasudevan, W. Jones, Q. Liu, J. Krollik, and L. Carin, "Electromagnetic time-reversal imaging of a target in a cluttered environment," *IEEE Trans. Ant. Prop.* **53**(9), pp. 3058–3066, 2005.

[41] A. Devaney, "Time reversal imaging of obscured targets from multistatic data," *IEEE Trans. Ant. Prop.* **53**(5), pp. 1600–1610, 2005.

[42] P. Kosmas and C. M. Rappaport, "A matched-filter fdtd-based time reversal approach for microwave breast cancer detection," *IEEE Trans. Ant. and Prop.* **54**(4), pp. 1257–1264, 2006.

[43] P. Blomgren, G. Papanicolaou, and H. Zhao, "Super-resolution in time-reversal acoustics," *J. Acoust. Soc. Am.* **111**(1), pp. 203–248, 2002.

[44] C. Oestges, A. D. Kim, G. Papanicolaou, and A. Paulraj, "Characterization of space-time focusing in time reversed random fields," *IEEE Trans. Ant. and Prop.* **53**(1), pp. 283–293, 2005.

[45] G. Papanicolaou, L. Ryzhik, and K. Solna, "Statistical stability in time reversal," *SIAM J. Appl. Math.* **64**, pp. 1133–1155, 2004.

[46] J. H. Taylor, *Scattering Theory*, Wiley, New York, 1972.

[47] T. Varslot, B. Yazıcı, and M. Cheney, "Wide-band pulse-echo imaging with distributed apertures in multi-path environments," *Inverse Problems* **24**, pp. 1–28, 2008.

[48] T. K. Sarkar, Z. Ji, K. Kim, A. Medouri, and M. Salazar-Palma, "A survey of various propagation models for mobile communication," *IEEE Ant. and Prop. Magazine* **45**, pp. 51–82, June 2003.

[49] A. T. Bharucha-Reid, *Random integral equations*, vol. 96 of *Mathematics in Science and Engineering*, Academic Press, New York, 1972.

[50] J. Weidmann, *Lineor Operotors in Hilbert Spaces*, Springer-Verlag, New York, 1980.

[51] B. Yazıcı, M. Cheney, and C. E. Yarman, "Synthetic aperture inversion for an arbitrary flight trajectory in the presence of noise and clutter," *Inverse Problems* **22**(5), pp. 1705–1729, 2006.

[52] J. Guerci, *Space-Time Adoptive Processing*, Artech House, Northwood, MA (USA), 2003.

APPENDIX

A. The Hilbert-Schmidt Norm

Let H_1 and H_2 be two Hilbert spaces. Furthermore, let $\{e^k\}$ be an orthonormal basis for H_1, and denote the inner-products